Evolution from γ-soft to stable triaxiality in ^{136}Nd as a prerequisite of chirality

B. F. Lv,[1,2] C. M. Petrache,[1,*] A. Astier,[1] E. Dupont,[1] A. Lopez-Martens,[1] P. T. Greenlees,[3] H. Badran,[3] T. Calverley,[3,4]
D. M. Cox,[3,5] T. Grahn,[3] J. Hilton,[3,4] R. Julin,[3] S. Juutinen,[3] J. Konki,[3,6] M. Leino,[3] J. Pakarinen,[3] P. Papadakis,[3,7] J. Partanen,[3]
P. Rahkila,[3] M. Sandzelius,[3] J. Saren,[3] C. Scholey,[3] J. Sorri,[3,8] S. Stolze,[3] J. Uusitalo,[3] A. Herzán,[9] B. Cederwall,[10]
A. Ertoprak,[10] H. Liu,[10] S. Guo,[2] M. L. Liu,[2] Y. H. Qiang,[2,11,12] J. G. Wang,[2] X. H. Zhou,[2] I. Kuti,[13] J. Timár,[13]
A. Tucholski,[14] J. Srebrny,[14] and C. Andreoiu[15]

[1]*Centre de Sciences Nucléaires et Sciences de la Matière, CNRS/IN2P3, Université Paris-Saclay, Bâtiment 104-108, 91405 Orsay, France*
[2]*Institute of Modern Physics, Chinese Academy of Sciences, Lanzhou 730000, China*
[3]*University of Jyväskylä, Department of Physics, FIN-40014 Jyväskylä, Finland*
[4]*Department of Physics, University of Liverpool, The Oliver Lodge Laboratory, Liverpool L69 7ZE, United Kingdom*
[5]*Department of Mathematical Physics, Lund Institu of Technology, S-22362 Lund, Sweden*
[6]*CERN, CH-1211 Geneva 23, Switzerland*
[7]*Oliver Lodge Laboratory, University of Liverpool, Liverpool L69 7ZE, United Kingdom*
[8]*Sodankylä Geophysical Observatory, University of Oulu, FIN-90014 Oulu, Finland*
[9]*Institute of Physics, Slovak Academy of Sciences, SK-84511 Bratislava, Slovakia*
[10]*KTH Department of Physics, S-10691 Stockholm, Sweden*
[11]*School of Nuclear Science and Technology, Lanzhou University, Lanzhou 730000, China*
[12]*Graduate University of Chinese Academy of Sciences, Beijing 000049, China*
[13]*Hungarian Academy of Sciences, Institute of Nuclear Research, 4001 Debrecen, Hungary*
[14]*University of Warsaw, Heavy Ion Laboratory, Pasteura 5a, 02-093 Warsaw, Poland*
[15]*Department of Chemistry, Simon Fraser University, Burnaby, British Columbia V5A 1S6, Canada*

The level structure of ^{136}Nd has been investigated using the ^{100}Mo(^{40}Ar, $4n$) reaction and the JUROGAM II+RITU+GREAT setup. The level scheme has been extended significantly. Many new bands have been identified both at low and high spin, among which are five nearly degenerate bands interpreted as chiral partners. Excitation energies, spins, and parities of the previously known bands are revised and firmly established, and some previously known bands have been revised. Configurations are assigned to the observed bands based on cranked Nilsson-Strutinsky calculations. The band structure of ^{136}Nd is now clarified and the various types of single-particle and collective excitations are well understood.

I. INTRODUCTION

The $A \approx 130$ mass region is among the most important areas of the nuclear landscape in which one can investigate the presence of triaxiality in deformed nuclei. Axial asymmetry was suggested for the ground states of nuclei in the region centered around $Z = 62$, $N = 76$ [1]. A regular increase of the level energies of the observed low-lying γ bands is considered a sign of rigid triaxiality, while a staggering of the level energies is considered a sign of soft triaxial shapes. Chirality, based on the relative spatial orientation of the nuclear deformation, the active single-particle orbits, and the collective rotational axis, is considered a fingerprint of triaxiality. It

was introduced to nuclear physics twenty year ago [2] and has been successfully employed to describe the observed nearly degenerate bands as rotation around an axis out of the three principal planes of the triaxial ellipsoidal shape. Nearly half of the chiral bands were observed in this region [3], widely supporting the existence of stable triaxial deformation. The studies of chirality in nuclei, both theoretical and experimental, suggested the coexistence of triaxial bands with different deformation parameters and revealed the associated phenomenon of multiple chiral doublets (MχD) [4–7]. The MχD phenomenon was first observed in ^{133}Ce [8]. Chiral partner bands are also expected to exist in even-even nuclei, but to achieve a stable chiral geometry, at least two pairs of nucleons should be broken, with at least one proton occupying a high-j quasiparticle orbital and one neutron occupying a high-j quasihole orbital. Comparing with neighboring odd-odd and odd-A nuclei, higher excitation energies are therefore needed to populate chiral bands in even-even nuclei, and high efficiency arrays are needed, since much lower intensities are expected due to the competition from various configurations comprising at least four unpaired nucleons. The first

---

observation of chiral bands in even-even nuclei was reported very recently in ^{136}Nd [9] and discussed using the multi-j shell particle-rotor model in Ref. [10].

Another type of collective motion uniquely associated with a triaxial nucleus, the wobbling mode, was also recently reported in ^{135}Pr [11]. However, the interpretation of the claimed wobbling band as transverse wobbling [12] was recently questioned in Ref. [13] and therefore remains unclear.

At medium spin, the nuclear shape can change under the polarizing effect of unpaired nucleons resulting from broken pairs. In certain cases the triaxial shape becomes more rigid, being based on a deeper minimum of the potential energy surface, induced by the protons occupying low-Ω orbitals in the lower part of the $h_{11/2}$ subshell, or by neutrons excited from orbitals below $N = 82$ to low-Ω ($h_{9/2}$, $f_{7/2}$) orbitals lying above $N = 82$ (see, e.g., [14,15] and references therein). In nuclei with several holes in the $N = 82$ shell closure, a multitude of triaxial bands have been observed in several Ce and Nd nuclei, giving strong support for the existence of stable triaxial shape up to very high spins in this mass region [14–24].

In addition to triaxial shapes, nuclei of this mass region can acquire other coexisting shapes at high spin, such as spherical, axially deformed, highly deformed, and even superdeformed. This is the case for ^{140}Nd, in which states based on a spherical shape have been observed up to spins as high as $27\hbar$ coexisting with triaxial shapes [25], and in which axial superdeformed and highly deformed shapes coexist at very high spin. In this nucleus, the bridge between the regions of highly deformed bands present in $A \approx 130$ nuclei and the superdeformed bands present in $A \approx 150$ nuclei is realized [26]. Highly deformed bands have been observed at medium to very high spin in several Nd nuclei [14,20–24,27–49]. Superdeformed bands have been observed in Ce nuclei [38,50–63].

In several nuclei the shape can become oblate at medium spins, when neutrons from the upper part of the $h_{11/2}$ subshell are active [64–69]. Of particular interest is a new collective rotational band observed in ^{137}Nd, which develops up to spin $I = 75/2\hbar$ and $E_x \approx 4.6$ MeV above yrast, being the first evidence of an oblate deformed nucleus rotating up to very high spin [70].

This region of the nuclear chart is therefore an ideal testing ground to investigate the competition between various deformations and their evolution with spins, as well as the competition between single-particle and collective modes of excitation. To achieve such studies, which tend towards complete spectroscopy, high efficiency experimental setups and high statistics are necessary.

The present work is devoted to refining the spectroscopy of ^{136}Nd, which is the nearest even-even neighbor of the first chiral candidate ^{134}Pr [2] and the first reported wobbler ^{135}Pr outside of the $A \approx 160$ region [11]. Located near the center of the triaxial region, this nucleus has been investigated in several previous experiments [43–45,71–80] and in theoretical works published in Refs. [81–85]. However, most of the experimental results were reported more than twenty years ago, and only a limited level scheme had been established prior to this work.

In this article, we report new experimental results on the extremely abundant structures in ^{136}Nd populated via the ^{100}Mo(^{40}Ar, 4n)^{136}Nd reaction. The high-quality data allow us to extend the level scheme of ^{136}Nd significantly. Partial results of this work on the newly observed chiral bands were reported in Ref. [9]. Sections II and III contain the description of the experiment and the data analysis. The structure of various bands is discussed in Sec. IV within the cranked Nilsson-Strutinski (CNS) framework as described in Refs. [86–89].

II. EXPERIMENTAL DETAILS

High-spin states in ^{136}Nd were populated using the ^{100}Mo(^{40}Ar, 4n) reaction at a beam energy of 152 MeV, provided by the K130 Cyclotron at the University of Jyväskylä, Finland. We used as target a self-supporting enriched ^{100}Mo foil of 0.5 mg/cm^2 thickness. The ^{135}Nd and ^{136}Nd nuclei were the most strongly populated in the reaction, with cross sections of around 100 mb each.

The JUROGAM II array [90], consisting of 24 clover and 15 coaxial tapered detectors placed at the target position, was used to detect prompt γ rays. The clover detectors were placed on two rings at 75.5° (12 clovers) and 104.5° (12 clovers), symmetric with respect to 90°. The tapered detectors were also placed on two rings at 133.6° (10 detectors) and 157.6° (5 detectors). The high-efficiency gas-filled recoil separator RITU [91] was coupled to the JUROGAM II array. After a flight time of about 650 ns in the RITU separator, the reaction residues were implanted in the GREAT focal plane detector array [92]. The GREAT detector array was composed of several detectors: A multiwire proportional counter (MWPC) measured the position of the recoils and delivered the time reference for the delayed γ-γ coincidences and for the time of flight of the recoils between the MWPC and a double-sided silicon strip detector (DSSD). The DSSD was also used to measure the decays of the implanted recoils. Behind the DSSD, a planar Ge strip detector was mounted to measure x rays and low-energy γ rays. For the measurement of high-energy γ-rays, three clover detectors were placed around the focal plane reaction chamber.

A total of 5.1×10^{10} prompt γ-ray coincidence events with fold $\geqslant 3$ were collected without any recoil gate. All the data were recorded by the triggerless Total Data Readout (TDR) data acquisition [93] and the events were time-stamped using a 100 MHz clock. The data were sorted using the GRAIN analysis package [94]. Fully symmetrized, three-dimensional (E_γ-E_γ-E_γ) and four-dimensional (E_γ-E_γ-E_γ-E_γ) matrices were analyzed using the RADWARE [95,96] analysis package.

The multipolarities of the γ rays were extracted using the directional correlation from oriented states (DCO) ratios (R_{DCO}) and two-point angular correlation (anisotropy) ratios R_{ac} [97,98].

The values of R_{ac} were extracted from γ-γ matrices, which were formed by sorting prompt coincidence events with combinations of 133.6° and 157.6° versus all angles and of 75.5° and 104.5° versus all angles, by setting the same energy gates on the all-angles projection spectrum in both matrices, and projecting on the other axis. Then, the R_{ac} ratio was calculated using the extracted intensities of the γ rays of interest (I_γ)

TABLE I. Experimental information including the γ-ray energies, energies of the initial levels E_i, intensities I_γ, anisotropies R_{DCO} and/or R_{ac}, multipolarities, and the spin-parity assignments to the observed states in ^{136}Nd. The transitions listed with increasing energy are grouped in bands. The deduced values for R_{DCO} with a stretched quadrupole gate are ≈ 1 for stretched quadrupole and ≈ 0.46 for dipole transitions, while the ratio is close to 1 for a dipole and 2.1 for a quadrupole transition when the gate is set on a dipole transition. The R_{ac} values for stretched dipole and quadrupole transitions are ≈ 0.8 and ≈ 1.4.

γ-ray energy[a]	E_i (keV)	Intensity[b]	R_{DCO}[c]	R_{ac}[d]	Multipolarity	$J_i^\pi \to J_f^\pi$
GSB						
373.7	373.7	100.0	1.01(5)[e]		$E2$	$2^+ \to 0^+$
602.5	976.2	91(5)	1.06(11)[e]		$E2$	$4^+ \to 2^+$
770.2	1746.4	80(7)	0.97(9)[e]		$E2$	$6^+ \to 4^+$
886.3	2632.7	56(4)	1.01(15)[e]		$E2$	$8^+ \to 6^+$
920.1	3552.8	14(2)	0.99(16)[e]		$E2$	$10^+ \to 8^+$
γ band						
182.7	2227.8	0.25(2)		0.73(21)	$M1$	$6^+ \to 5^+$
191.9	2227.8	0.12(2)			$E1$	$6^+ \to 5^-$
368.7	1230.9	0.8(2)		1.10(25)	$M1/E2$	$3^+ \to 2^+$
488.5	862.2	1.7(3)		1.43(31)	$E2$	$2^+ \to 2^+$
490.3	3768.0	0.32(4)	0.71(9)[e]		$M1/E2$	$10^+ \to 10^+$
551.7	4319.7	2.7(2)	1.13(14)[e]		$E2$	$12^+ \to 10^+$
565.5	1541.7	1.3(4)		1.07(45)	$M1/E2$	$4^+ \to 4^+$
600.4	3768.0	0.7(2)	1.1(4)[e]		$E2$	$10^+ \to 8^+$
679.5	1541.7	1.8(3)	1.05(25)[e]		$E2$	$4^+ \to 2^+$
686.1	2227.8	0.71(6)		1.3(2)	$E2$	$6^+ \to 4^+$
711.8	5031.5	4.0(3)	1.08(17)[e]		$E2$	$14^+ \to 12^+$
725.7	5757.2	2.1(2)			$E2$	$16^+ \to 14^+$
735.2	5757.2	2.7(2)	1.1(2)[e]		$E2$	$16^+ \to 14^+$
766.9	4319.7	7.7(7)	1.0(2)[e]		$E2$	$12^+ \to 10^+$
811.0	2352.7	1.3(2)		1.38(23)	$E2$	$6^+ \to 4^+$
814.2	2045.1	6.5(6)		1.31(20)	$E2$	$5^+ \to 3^+$
814.9	3167.6	0.92(8)	1.05(15)[e]		$E2$	$8^+ \to 6^+$
844.8	6602.0	1.8(2)	0.98(25)[e]		$E2$	$18^+ \to 16^+$
857.2	1230.9	6.1(6)		1.16(15)	$M1/E2$	$3^+ \to 2^+$
862.2	862.2	1.5(3)	1.1(3)[e]		$E2$	$2^+ \to 0^+$
907.1	6602.0	0.12(1)			$E2$	$18^+ \to 16^+$
1017.7	7619.7	0.83(5)	1.02(18)[e]		$E2$	$20^+ \to 18^+$
1135.3	3768.0	1.9(3)	0.98(25)[e]		$E2$	$10^+ \to 8^+$
1162.7	6602.0	0.21(2)			$E2$	$18^+ \to 16^+$
1251.6	2227.8	0.31(3)		1.41(26)	$E2$	$6^+ \to 4^+$
1410.7	6602.0	0.12(3)			$E2$	$18^+ \to 16^+$
1410.8	5757.2	0.11(2)			$E2$	$16^+ \to 14^+$
1428.6	7619.7	0.15(2)			$E2$	$20^+ \to 18^+$
Band N1						
163.6	2757.3	0.05(1)			$M1/E2$	$8^- \to 7^-$
183.1	2940.4	0.65(8)		0.86(15)	$M1$	$9^- \to 8^-$
255.6	2483.4	0.65(5)		0.73(13)	$E1$	$6^- \to 6^+$
273.9	2757.3	4.1(4)	1.02(15)[e]		$E2$	$8^- \to 6^-$
302.8	3243.2	0.9(1)	0.42(8)[e]		$M1$	$10^- \to 9^-$
307.7	2940.4	1.1(3)	0.45(15)[e]		$E1$	$9^- \to 8^+$
317.7	2757.3	4.7(4)	0.54(7)[e]		$M1$	$8^- \to 7^-$
358.1	3601.3	0.72(8)		1.21(15)	$M1/E2$	$11^- \to 10^-$
403.7	2439.6	6.4(3)	0.99(8)[e]		$E2$	$7^- \to 5^-$
410.0	6903.2	0.18(4)			$E2$	$19^- \to 17^-$
410.7	4425.7	0.16(4)	0.42(11)[e]		$M1$	$13^- \to 12^-$
411.8	2757.3	0.7(1)		1.45(35)	$E2$	$8^- \to 6^-$
413.7	4015.0	0.10(2)			$M1/E2$	$12^- \to 11^-$
438.3	2483.4	1.24(7)		0.86(6)	$E1$	$6^- \to 5^+$
447.5	2483.4	1.6(2)		0.84(12)	$M1$	$6^- \to 5^-$

TABLE I. (*Continued.*)

γ-ray energy[a]	E_i (keV)	Intensity[b]	R_{DCO}[c]	R_{ac}[d]	Multipolarity	$J_i^\pi \to J_f^\pi$
485.9	3243.2	3.6(4)		1.31(15)	$E2$	$10^- \to 8^-$
501.3	2940.4	20(1)	1.06(8)[e]		$E2$	$9^- \to 7^-$
660.9	3601.3	8(1)	1.0(1)[e]		$E2$	$11^- \to 9^-$
693.2	2439.6	21(2)	0.61(13)[e]		$E1$	$7^- \to 6^+$
737.0	2483.4	2.3(3)		1.07(20)	$E1$	$6^- \to 6^+$
743.8	6844.0	0.15(1)			$E2$	$18^- \to 16^-$
771.8	4015.0	3.3(3)		1.4(2)	$E2$	$12^- \to 10^-$
824.4	4425.7	2.7(3)	1.03(15)[e]		$E2$	$13^- \to 11^-$
832.0	7676.0	0.09(2)			$E2$	$(20^-) \to 18^-$
989.4	5415.1	2.2(2)	1.06(14)[e]		$E2$	$15^- \to 13^-$
1005.9	5020.9	2.5(3)	0.97(15)[e]		$E2$	$14^- \to 12^-$
1059.7	2035.9	9.3(8)	0.64(11)[e]		$E1$	$5^- \to 4^+$
1076.9	6492.0	0.47(4)	1.04(22)[e]		$E2$	$17^- \to 15^-$
1079.3	6100.2	0.31(2)		1.32(30)	$E2$	$16^- \to 14^-$
Band N2						
154.1	2593.7	0.21(2)		0.7(2)	$M1$	$7^- \to 7^-$
248.2	2593.7	2.6(2)		0.68(12)	$M1$	$7^- \to 6^-$
300.4	2345.5	4.7(3)		0.81(7)	$E1$	$6^- \to 5^+$
316.2	2909.9	0.41(2)	0.87(17)[f]		$M1/E2$	$8^- \to 7^-$
337.0	3246.9	0.71(2)	0.63(7)[f]		$M1/E2$	$9^- \to 8^-$
365.9	2593.7	0.73(3)		0.71(13)	$E1$	$7^- \to 6^+$
465.3	3712.2	0.29(2)	0.61(5)[f]		$M1/E2$	$10^- \to 9^-$
564.4	2909.9	1.1(1)		1.40(18)	$E2$	$8^- \to 6^-$
653.2	3246.9	3.7(2)		1.40(8)	$E2$	$9^- \to 7^-$
802.3	3712.2	0.63(3)	1.97(11)[f]		$E2$	$10^- \to 8^-$
847.3	2593.7	0.94(5)		0.86(6)	$E1$	$7^- \to 6^+$
869.1	4116.0	3.0(2)	2.13(23)[f]		$E2$	$11^- \to 9^-$
904.2	4616.4	0.41(8)	2.17(45)[f]		$E2$	$12^- \to 10^-$
988.9	5104.9	1.47(6)	2.21(14)[f]		$E2$	$13^- \to 11^-$
1068.0	5684.4	0.22(1)	2.0(3)[f]		$E2$	$14^- \to 12^-$
Band L1						
123.7	3295.7	0.5(1)	0.47(12)[e]		$E1$	$10^+ \to 9^-$
355.3	3295.7	9.7(3)	0.58(8)[e]		$E1$	$10^+ \to 9^-$
389.9	3685.6	34(2)	1.01(20)[e]		$E2$	$12^+ \to 10^+$
414.7	3172.0	0.63(5)	0.45(12)[e]		$M1$	$9^- \to 8^-$
660.8	4346.4	23(2)	1.1(1)[e]		$E2$	$14^+ \to 12^+$
663.0	3295.7	30(3)	1.12(24)[e]		$E2$	$10^+ \to 8^+$
732.4	3172.0	0.55(2)	1.08(13)[e]		$E2$	$9^- \to 7^-$
844.9	5191.3	12.2(7)	1.10(16)[e]		$E2$	$16^+ \to 14^+$
883.1	7354.9	0.41(5)		1.5(2)	$E2$	$20^+ \to 18^+$
999.8	6191.1	5.7(4)	1.07(15)[e]		$E2$	$18^+ \to 16^+$
1163.8	7354.9	1.13(9)		1.47(24)	$E2$	$20^+ \to 18^+$
1268.7	8623.6	0.65(4)		1.53(21)	$E2$	$22^+ \to 20^+$
1378.2	10001.8	0.10(1)			$E2$	$(24^+) \to 22^+$
1492.3	11494.1	0.05(1)			$E2$	$(26^+) \to (24^+)$
Band L2						
663.4	5694.9	1.9(2)	1.12(16)[e]		$E2$	$16^+ \to 14^+$
672.9	5694.9	3.3(2)	1.04(20)[e]		$E2$	$16^+ \to 14^+$
702.3	5022.0	6.1(3)	1.13(17)[e]		$E2$	$14^+ \to 12^+$
789.5	6546.7	0.31(2)		1.46(29)	$E2$	$18^+ \to 16^+$
851.8	6546.7	1.5(3)	1.03(30)[e]		$E2$	$18^+ \to 16^+$
976.7	6546.7	<0.01			$E2$	$18^+ \to 16^+$
1044.7	7591.4	0.43(2)		1.44(25)	$E2$	$20^+ \to 18^+$
Band L3						
487.3	4454.0	0.10(5)			$E2$	$13^+ \to 11^+$
678.5	5131.6	0.63(7)		1.33(23)	$E2$	$15^+ \to 13^+$

TABLE I. (*Continued.*)

γ-ray energy[a]	E_i (keV)	Intensity[b]	R_{DCO} [c]	R_{ac} [d]	Multipolarity	$J_i^\pi \rightarrow J_f^\pi$
739.9	6931.0	0.52(4)		0.63(12)	$M1$	$19^+ \rightarrow 18^+$
750.7	5942.0	1.75(6)	0.46(6)[e]		$M1$	$17^+ \rightarrow 16^+$
768.4	4454.0	1.8(3)		1.54(50)	$M1/E2$	$13^+ \rightarrow 12^+$
785.2	5131.6	1.9(1)	0.58(12)[e]		$M1/E2$	$15^+ \rightarrow 14^+$
810.4	5942.0	1.35(8)	0.98(9)[e]		$E2$	$17^+ \rightarrow 15^+$
989.0	6931.0	1.5(1)	1.01(15)[e]		$E2$	$19^+ \rightarrow 17^+$
1168.8	8099.8	0.34(3)		1.37(24)	$E2$	$21^+ \rightarrow 19^+$
Band L4						
401.6	4855.6	0.35(2)		1.05(23)	$M1/E2$	$14^+ \rightarrow 13^+$
438.4	5570.0	0.42(3)		0.77(14)	$M1$	$16^+ \rightarrow 15^+$
518.6	4855.6	0.41(2)			$E2$	$14^+ \rightarrow 12^+$
714.4	5570.0	1.43(7)	0.97(13)[e]		$E2$	$16^+ \rightarrow 14^+$
784.2	4337.0	0.38(2)		1.33(25)	$E2$	$12^+ \rightarrow 10^+$
901.8	6471.8	3.1(2)	1.05(18)[e]		$E2$	$18^+ \rightarrow 16^+$
1001.3	7473.1	0.57(4)	1.1(2)[e]		$E2$	$20^+ \rightarrow 18^+$
1041.3	4337.0	0.7(2)	1.12(27)[e]		$E2$	$12^+ \rightarrow 10^+$
1088.4	8560.0	0.21(2)		1.49(29)	$E2$	$22^+ \rightarrow 20^+$
1170.0	4855.6	1.23(6)	1.11(19)[e]		$E2$	$14^+ \rightarrow 12^+$
1223.6	5570.0	2.5(2)	0.97(13)[e]		$E2$	$16^+ \rightarrow 14^+$
1276.7	8249.8	0.17(2)		1.5(2)	$E2$	$22^+ \rightarrow 20^+$
1280.4	6471.8	0.58(5)	1.10(20)[e]		$E2$	$18^+ \rightarrow 16^+$
Band L5						
275.1	7141.5	0.11(1)	0.47(9)[e]		$E1$	$19^- \rightarrow 19^+$
467.4	7141.5	0.03(1)			$M1/E2$	$19^- \rightarrow 18^-$
518.1	8049.5	<0.01			$M1/E2$	$21^- \rightarrow 20^-$
781.4	7141.5	1.5(1)	1.03(19)[e]		$E2$	$19^- \rightarrow 17^-$
908.0	8049.5	1.35(11)	0.94(12)[e]		$E2$	$21^- \rightarrow 19^-$
945.0	6360.1	1.15(9)	1.07(24)[e]		$E2$	$17^- \rightarrow 15^-$
950.4	7141.5	1.11(7)	0.53(10)[e]		$E1$	$19^- \rightarrow 18^+$
984.9	9048.4	0.30(2)		1.37(21)	$E2$	$23^- \rightarrow 21^-$
998.9	9048.4	0.40(4)	1.0(2)[e]		$E2$	$23^- \rightarrow 21^-$
1168.8	6360.1	0.53(5)	0.49(8)[e]		$E1$	$17^- \rightarrow 16^+$
Band L6						
390.1	7531.4	0.10(5)			$M1/E2$	$20^- \rightarrow 19^-$
635.2	6674.1	1.3(1)	1.03(15)[e]		$E2$	$18^- \rightarrow 16^-$
847.6	6038.9	0.31(1)	0.47(12)[e]		$E1$	$16^- \rightarrow 16^+$
857.3	7531.4	1.23(14)	0.98(22)[e]		$E2$	$20^- \rightarrow 18^-$
860.0	8536.0	0.05(1)			$E2$	$22^- \rightarrow 20^-$
1004.6	8536.0	1.1(1)	1.01(18)[e]		$E2$	$22^- \rightarrow 20^-$
1018.0	6038.9	1.1(2)	1.03(37)[e]		$E2$	$16^- \rightarrow 14^-$
Band L7						
645.0	3277.7	7.5(6)	1.04(12)[e]		$E2$	$10^+ \rightarrow 8^+$
718.3	3996.0	4.6(3)	1.05(20)[e]		$E2$	$12^+ \rightarrow 10^+$
851.6	4848.6	2.9(2)	1.02(15)[e]		$E2$	$14^+ \rightarrow 12^+$
995.2	5842.8	1.63(17)		1.52(26)	$E2$	$16^+ \rightarrow 14^+$
Band L8						
342.7	6929.5	0.11(1)		0.71(22)	$M1$	$18^+ \rightarrow 17^+$
350.0	6929.5	0.45(4)	0.72(15)[f]		$M1/E2$	$18^+ \rightarrow 17^+$
743.5	6586.3	0.34(2)		0.64(16)	$M1$	$17^+ \rightarrow 16^+$
841.0	4837.0	0.48(3)		0.68(9)	$M1$	$13^+ \rightarrow 12^+$
859.7	6586.3	0.19(4)		1.58(45)	$E2$	$17^+ \rightarrow 15^+$
879.0	5726.6	0.58(2)		1.21(25)	$M1/E2$	$15^+ \rightarrow 14^+$
889.6	5726.6	0.19(2)		1.5(3)	$E2$	$15^+ \rightarrow 13^+$
Band L9						
438.7	7732.3	0.13(5)			$M1/E2$	$20^+ \rightarrow 19^+$

TABLE I. (*Continued.*)

γ-ray energy[a]	E_i (keV)	Intensity[b]	R_{DCO}[c]	R_{ac}[d]	Multipolarity	$J_i^\pi \rightarrow J_f^\pi$
743.9	8794.3	0.05(1)			$M1/E2$	$22^+ \rightarrow 21^+$
912.1	6754.9	0.74(3)		1.49(23)	$E2$	$18^+ \rightarrow 16^+$
977.4	7732.3	0.20(1)		1.43(25)	$E2$	$20^+ \rightarrow 18^+$
1062.3	8794.3	0.10(1)		1.44(22)	$E2$	$22^+ \rightarrow 20^+$
Band D1						
219.9	4665.9	0.82(6)	0.95(9)[f]		$M1$	$12^+ \rightarrow 11^+$
254.1	4920.0	1.72(15)	0.48(11)[e]		$M1$	$13^+ \rightarrow 12^+$
293.8	5213.8	1.42(8)	0.71(7)[e]		$M1$	$14^+ \rightarrow 13^+$
328.9	4665.9	0.30(3)	1.24(29)[f]		$M1/E2$	$12^+ \rightarrow 12^+$
345.3	5559.1	1.1(1)	0.66(9)[f]		$M1/E2$	$15^+ \rightarrow 14^+$
411.1	5970.2	0.75(4)	0.98(10)[f]		$M1$	$16^+ \rightarrow 15^+$
453.8	6424.0	0.37(9)	0.81(25)[f]		$M1/E2$	$17^+ \rightarrow 16^+$
479.3	4446.0	0.13(2)		0.83(17)	$M1$	$11^+ \rightarrow 11^+$
485.0	6909.0	0.23(3)	0.94(20)[f]		$M1/E2$	$18^+ \rightarrow 17^+$
583.0	4920.0	0.11(1)			$M1/E2$	$13^+ \rightarrow 12^+$
594.1	7503.1	0.14(2)		1.09(19)	$M1/E2$	$19^+ \rightarrow 18^+$
613.0	8116.1	0.05(2)			$M1/E2$	$20^+ \rightarrow 19^+$
618.7	7503.1	0.10(1)			$M1/E2$	$19^+ \rightarrow 18^+$
639.1	5559.1	0.04(2)			$E2$	$15^+ \rightarrow 13^+$
671.0	3966.7	0.8(1)	1.21(18)[f]		$M1/E2$	$11^+ \rightarrow 10^+$
699.2	4665.9	0.49(3)	1.1(3)[f]		$M1/E2$	$12^+ \rightarrow 11^+$
756.4	5970.2	0.06(3)			$E2$	$16^+ \rightarrow 14^+$
844.7	4446.0	0.09(1)			$(E1)$	$11^+ \rightarrow 11^-$
864.9	6424.0	0.25(10)			$E2$	$17^+ \rightarrow 15^+$
905.0	4920.0	0.15(2)			$(E1)$	$13^+ \rightarrow 12^-$
980.3	4665.9	0.16(3)	1.60(45)[f]		$M1/E2$	$12^+ \rightarrow 12^+$
1064.6	4665.9	0.26(4)	1.16(36)[f]		$E1$	$12^+ \rightarrow 11^-$
1150.3	4446.0	0.62(6)		0.81(8)	$M1$	$11^+ \rightarrow 10^+$
1202.8	4446.0	0.05(1)			$(E1)$	$11^+ \rightarrow 10^-$
1234.4	4920.0	0.12(3)			$M1/E2$	$13^+ \rightarrow 12^+$
Band D-chiral						
431.7	6485.4	0.15(5)		0.93(50)	$M1/E2$	$17^+ \rightarrow 16^+$
503.9	6989.3	<0.01			$M1/E2$	$18^+ \rightarrow 17^+$
515.2	6485.4	0.11(3)		0.73(28)	$M1$	$17^+ \rightarrow 16^+$
716.4	5636.4	0.03(2)			$E2$	$15^+ \rightarrow 13^+$
839.9	6053.7	0.22(4)		1.4(3)	$E2$	$16^+ \rightarrow 14^+$
1019.1	6989.3	0.10(3)		1.43(32)	$E2$	$18^+ \rightarrow 16^+$
1045.2	7469.2	0.12(2)		1.31(29)	$E2$	$19^+ \rightarrow 17^+$
Band D2						
117.9	6347.9	0.25(10)	0.72(37)[f]		$M1/E2$	$16^+ \rightarrow 15^+$
231.1	6579.0	0.89(6)		0.78(7)	$M1$	$17^+ \rightarrow 16^+$
298.1	6884.4	0.11(1)		0.86(15)	$M1$	$18^+ \rightarrow 17^+$
305.4	6884.4	1.41(15)		1.06(20)	$M1/E2$	$18^+ \rightarrow 17^+$
318.3	8050.6	0.21(2)		1.10(14)	$M1/E2$	$21^+ \rightarrow 20^+$
364.6	7293.6	0.50(4)	1.17(18)[f]		$M1$	$19^+ \rightarrow 18^+$
376.4	7670.0	1.9(3)	1.54(60)[f]		$M1/E2$	$20^+ \rightarrow 19^+$
380.6	8050.6	1.4(2)		0.85(12)	$M1$	$21^+ \rightarrow 20^+$
384.6	7293.6	0.12(2)	1.02(17)[f]		$M1$	$19^+ \rightarrow 18^+$
409.2	7293.6	1.72(9)	0.84(8)[f]		$M1/E2$	$19^+ \rightarrow 18^+$
416.3	8466.9	1.15(3)	0.98(9)[f]		$M1$	$22^+ \rightarrow 21^+$
460.4	6884.4	0.21(1)		1.16(13)	$M1/E2$	$18^+ \rightarrow 17^+$
481.2	8948.1	0.89(4)	0.88(9)[f]		$M1/E2$	$23^+ \rightarrow 22^+$
543.3	9491.4	0.52(1)	1.15(15)[f]		$M1$	$24^+ \rightarrow 23^+$
600.0	10091.4	0.37(10)			$M1/E2$	$25^+ \rightarrow 24^+$
671.8	10763.2	0.27(4)	0.85(22)[f]		$M1/E2$	$26^+ \rightarrow 25^+$
736.2	6579.0	0.55(4)		1.13(18)	$M1/E2$	$17^+ \rightarrow 16^+$

TABLE I. (*Continued.*)

γ-ray energy[a]	E_i (keV)	Intensity[b]	R_{DCO}[c]	R_{ac}[d]	Multipolarity	$J_i^{\pi} \rightarrow J_f^{\pi}$
785.6	7670.0	0.08(2)			$E2$	$20^+ \rightarrow 18^+$
852.4	6579.0	0.5(2)		1.3(4)	$E2$	$17^+ \rightarrow 15^+$
914.2	6884.4	0.15(2)			$E2$	$18^+ \rightarrow 16^+$
942.0	4938.0	0.35(5)		0.8(2)	$M1$	$13^+ \rightarrow 12^+$
1292.0	6230.0	0.17(3)		1.41(42)	$E2$	$15^+ \rightarrow 13^+$
1393.0	6230.0	0.10(2)			$E2$	$15^+ \rightarrow 13^+$
1382.4	6230.0	0.14(2)		1.0(3)	$M1/E2$	$15^+ \rightarrow 14^+$
Band D2-chiral						
408.7	9248.7	0.10(3)		1.25(40)	$M1/E2$	$23^+ \rightarrow 22^+$
(426.0)	8840.0	<0.01			$M1/E2$	$22^+ \rightarrow 21^+$
447.2	9695.9	<0.02			$M1/E2$	$24^+ \rightarrow 23^+$
453.1	10659.2	0.04(1)			$M1/E2$	$26^+ \rightarrow 25^+$
510.2	10206.1	0.05(2)			$M1/E2$	$25^+ \rightarrow 24^+$
599.4	11258.6	0.05(2)			$M1/E2$	$27^+ \rightarrow 26^+$
1120.4	8414.0	0.14(3)		1.31(42)	$E2$	$21^+ \rightarrow 19^+$
1167.2	11258.6	0.10(3)		1.42(60)	$E2$	$27^+ \rightarrow 25^+$
1167.8	10659.2	0.03(2)			$E2$	$26^+ \rightarrow 24^+$
1170.0	8840.0	0.18(4)		1.4(3)	$E2$	$22^+ \rightarrow 20^+$
1198.1	9248.7	0.15(3)		1.37(50)	$E2$	$23^+ \rightarrow 21^+$
1229.0	9695.9	0.10(3)		1.40(45)	$E2$	$24^+ \rightarrow 22^+$
1258.0	10206.1	0.05(1)			$E2$	$25^+ \rightarrow 23^+$
Band D3						
134.2	5732.2	0.13(1)		0.76(13)	$M1$	$15^- \rightarrow 14^-$
183.1	5532.1	1.64(7)		0.75(8)	$M1$	$14^- \rightarrow 13^-$
200.1	5732.2	1.53(15)	1.02(15)[f]		$M1/E2$	$15^- \rightarrow 14^-$
248.7	5980.9	1.33(10)	1.05(17)[f]		$M1$	$16^- \rightarrow 15^-$
292.0	5349.0	1.71(5)		0.79(5)	$M1$	$13^- \rightarrow 12^-$
333.4	5980.9	0.07(1)			$M1/E2$	$16^- \rightarrow 15^-$
345.4	6326.3	1.7(2)		0.74(11)	$M1$	$17^- \rightarrow 16^-$
355.1	5532.1	0.3(1)	1.14(43)[f]		$M1$	$14^- \rightarrow 13^-$
369.9	6326.3	0.23(1)			$M1/E2$	$17^- \rightarrow 16^-$
382.4	5980.9	1.03(7)	1.94(29)[f]		$E2$	$16^- \rightarrow 14^-$
383.2	5732.2	0.15(3)	1.9(4)[f]		$E2$	$15^- \rightarrow 13^-$
421.5	5598.5	0.31(1)		0.79(11)	$M1$	$14^- \rightarrow 13^-$
427.2	5532.1	0.05(1)			$M1/E2$	$14^- \rightarrow 13^-$
434.2	6760.5	1.23(9)	1.1(2)[f]		$M1$	$18^- \rightarrow 17^-$
447.3	6760.5	0.41(3)		0.8(1)	$M1$	$18^- \rightarrow 17^-$
448.8	8169.9	0.36(1)	1.07(17)[f]		$M1$	$21^- \rightarrow 20^-$
448.8	5980.9	0.27(12)			$E2$	$16^- \rightarrow 14^-$
465.7	7226.2	0.74(5)	1.19(18)[f]		$M1$	$19^- \rightarrow 18^-$
493.6	5598.5	0.42(3)		1.01(13)	$M1/E2$	$14^- \rightarrow 13^-$
494.9	7721.1	0.57(7)	0.92(12)[f]		$M1$	$20^- \rightarrow 19^-$
520.0	5349.0	0.35(4)		1.11(28)	$M1/E2$	$13^- \rightarrow 12^-$
520.2	8690.1	0.25(4)	1.28(27)[f]		$M1/E2$	$22^- \rightarrow 21^-$
542.0	9232.1	0.15(1)	1.6(3)[f]		$M1/E2$	$23^- \rightarrow 22^-$
555.1	9787.2	0.04(1)			$M1/E2$	$24^- \rightarrow 23^-$
557.0	5734.0	0.12(1)		1.1(1)	$M1/E2$	$14^- \rightarrow 13^-$
560.6	5177.0	<0.01			$M1/E2$	$13^- \rightarrow 12^-$
594.1	6326.3	0.27(2)		1.3(2)	$E2$	$17^- \rightarrow 15^-$
732.6	5349.0	0.09(1)			$M1/E2$	$13^- \rightarrow 12^-$
750.1	4027.8	2.36(20)		0.74(10)	$E1$	$11^- \rightarrow 10^+$
750.9	5598.5	0.58(3)	1.02(15)[f]		$M1$	$14^- \rightarrow 14^+$
801.2	4829.0	0.41(2)		0.77(14)	$M1$	$12^- \rightarrow 11^-$
943.7	8169.9	0.07(2)			$E2$	$21^- \rightarrow 19^-$
960.6	7721.1	0.08(3)			$E2$	$20^- \rightarrow 18^-$
1029.2	5057.0	1.95(4)		1.08(15)	$M1/E2$	$12^- \rightarrow 11^-$

TABLE I. (*Continued.*)

γ-ray energy[a]	E_i (keV)	Intensity[b]	R_{DCO}[c]	R_{ac}[d]	Multipolarity	$J_i^\pi \rightarrow J_f^\pi$
1061.0	5177.0	1.2(3)		1.1(3)	$M1/E2$	$13^- \rightarrow 12^-$
1097.1	9787.2	0.02(1)			$E2$	$24^- \rightarrow 23^-$
1185.7	5532.1	0.26(2)		0.92(25)	$E1$	$14^- \rightarrow 14^+$
1353.0	5349.0	0.4(1)		0.89(30)	$E1$	$13^- \rightarrow 12^+$
Band D3-chiral						
945.1	7271.4	0.21(5)		1.44(55)	$E2$	$19^- \rightarrow 17^-$
962.1	7722.6	0.11(5)		1.5(4)	$E2$	$20^- \rightarrow 18^-$
988.9	8215.1	0.07(2)		1.39(32)	$E2$	$21^- \rightarrow 19^-$
1030.6	8751.7	0.16(3)		1.35(26)	$E2$	$22^- \rightarrow 20^-$
Band D4						
224.2	5956.4	0.07(2)			$M1/E2$	$16^- \rightarrow 15^-$
229.7	5647.5	1.29(10)	0.75(10)[f]		$M1/E2$	$15^- \rightarrow 14^-$
275.7	5647.5	0.54(3)	0.77(5)[f]		$M1/E2$	$15^- \rightarrow 14^-$
308.9	5956.4	2.3(2)	0.48(8)[e]		$M1$	$16^- \rightarrow 15^-$
332.3	6313.2	0.77(5)		0.84(8)	$M1$	$17^- \rightarrow 16^-$
338.7	5647.5	0.82(7)	0.83(11)[f]		$M1/E2$	$15^- \rightarrow 14^-$
356.8	6313.2	1.7(2)	0.93(24)[f]		$M1$	$17^- \rightarrow 16^-$
388.7	6715.0	0.61(18)			$M1/E2$	$18^- \rightarrow 17^-$
401.8	6715.0	1.9(2)	1.09(19)[f]		$M1$	$18^- \rightarrow 17^-$
426.6	7577.7	1.1(1)	0.97(13)[f]		$M1$	$20^- \rightarrow 19^-$
436.1	7151.1	1.82(20)	0.45(6)[e]		$M1$	$19^- \rightarrow 18^-$
445.3	8023.0	0.88(10)	0.95(27)[f]		$M1$	$21^- \rightarrow 20^-$
487.6	8510.6	0.61(6)	1.17(29)[f]		$M1/E2$	$22^- \rightarrow 21^-$
510.0	9020.6	0.30(5)		0.73(21)	$M1$	$23^- \rightarrow 22^-$
538.6	5956.4	0.33(6)		1.39(42)	$E2$	$16^- \rightarrow 14^-$
541.3	5956.4	0.24(1)		1.16(18)	$M1/E2$	$16^- \rightarrow 15^-$
549.8	9570.4	0.21(2)		1.13(25)	$M1/E2$	$24^- \rightarrow 23^-$
630.8	10201.2	0.05(2)			$M1/E2$	$25^- \rightarrow 24^-$
665.7	6313.2	0.23(6)		1.32(33)	$E2$	$17^- \rightarrow 15^-$
745.7	4347.0	0.58(3)	0.51(11)[e]		$M1$	$12^- \rightarrow 11^-$
758.6	6715.0	0.3(1)	1.94(26)[f]		$E2$	$18^- \rightarrow 16^-$
784.7	4386.0	2.9(2)	0.51(7)[f]		$M1/E2$	$12^- \rightarrow 11^-$
837.9	7151.1	0.21(4)	1.83(38)[f]		$E2$	$19^- \rightarrow 17^-$
862.7	7577.7	0.17(4)	1.98(27)[f]		$E2$	$20^- \rightarrow 18^-$
871.9	8023.0	0.15(3)		1.42(36)	$E2$	$21^- \rightarrow 19^-$
883.1	5308.8	0.24(3)	1.13(16)[f]		$M1$	$14^- \rightarrow 13^-$
922.8	5308.8	0.61(5)	1.9(2)[f]		$E2$	$14^- \rightarrow 12^-$
932.9	8510.6	0.15(3)		1.33(31)	$E2$	$22^- \rightarrow 20^-$
961.8	5308.8	0.25(2)	1.97(24)[f]		$E2$	$14^- \rightarrow 12^-$
985.8	5371.8	0.81(4)	2.01(19)[f]		$E2$	$14^- \rightarrow 12^-$
997.6	9020.6	0.15(5)			$E2$	$23^- \rightarrow 21^-$
1031.8	5417.8	1.4(1)	1.91(20)[f]		$E2$	$14^- \rightarrow 12^-$
1059.8	9570.4	0.12(4)		1.4(3)	$E2$	$24^- \rightarrow 22^-$
1070.8	5417.8	0.33(2)		1.41(21)	$E2$	$14^- \rightarrow 12^-$
1180.6	10201.2	0.07(2)			$E2$	$25^- \rightarrow 23^-$
1221.8	5647.5	0.20(2)		1.38(18)	$E2$	$15^- \rightarrow 13^-$
Band D4-chiral						
945.0	7258.2	0.10(3)		1.36(45)	$E2$	$19^- \rightarrow 17^-$
1022.0	7737.0	0.25(4)		1.41(27)	$E2$	$20^- \rightarrow 18^-$
1059.9	8211.0	0.6(3)			$(E2)$	$21^- \rightarrow 19^-$
1050.3	8628.0	0.14(4)		1.26(37)	$E2$	$22^- \rightarrow 20^-$
1069.2	9092.2	0.10(2)		1.45(30)	$E2$	$23^- \rightarrow 21^-$
1172.4	9683.0	<0.01			$E2$	$24^- \rightarrow 22^-$
Band D5						
180.2	6006.2	0.17(3)		1.51(36)	$M1/E2$	$16^+ \rightarrow 15^+$
231.8	6238.0	1.8(2)	0.71(12)[f]		$M1/E2$	$17^+ \rightarrow 16^+$

TABLE I. (*Continued.*)

γ-ray energy[a]	E_i (keV)	Intensity[b]	R_{DCO} [c]	R_{ac} [d]	Multipolarity	$J_i^\pi \to J_f^\pi$
283.8	6521.8	2.5(4)	0.84(15)[f]		$M1/E2$	$18^+ \to 17^+$
319.7	6866.4	1.05(10)	0.39(8)[e]		$M1/E2$	$19^+ \to 18^+$
344.6	6866.4	5.9(4)		0.81(9)	$M1$	$19^+ \to 18^+$
388.2	7254.6	5(1)			$M1/E2$	$20^+ \to 19^+$
412.0	6238.0	0.15(5)		1.3(3)	$E2$	$17^+ \to 15^+$
429.7	7684.3	2.8(2)	0.86(13)[f]		$M1/E2$	$21^+ \to 20^+$
462.7	8147.0	1.5(1)	0.96(14)[f]		$M1$	$22^+ \to 21^+$
504.0	8651.0	1.1(1)	0.97(11)[f]		$M1$	$23^+ \to 22^+$
515.6	6521.8	0.35(10)	0.92(33)[e]		$E2$	$18^+ \to 16^+$
526.3	9177.3	0.47(5)		0.99(15)	$M1/E2$	$24^+ \to 23^+$
543.1	6238.0	0.72(3)	0.74(8)[e]		$M1/E2$	$17^+ \to 16^+$
567.1	9744.4	0.31(2)		0.74(16)	$M1$	$25^+ \to 24^+$
579.8	6521.8	1.01(8)	1.22(18)[f]		$M1/E2$	$18^+ \to 17^+$
599.6	10344.0	0.2(1)			$M1/E2$	$26^+ \to 25^+$
628.4	6866.4	1.3(2)	1.02(19)[e]		$E2$	$19^+ \to 17^+$
707.9	7254.6	0.25(3)		1.41(26)	$E2$	$20^+ \to 18^+$
732.8	7254.6	0.8(2)		1.4(3)	$E2$	$20^+ \to 18^+$
764.6	6521.8	1.9(2)	2.16(29)[f]		$E2$	$18^+ \to 16^+$
798.7	6238.0	0.81(7)	1.34(16)[e]		$M1/E2$	$17^+ \to 16^+$
817.9	7684.3	1.6(2)	2.39(35)[f]		$E2$	$21^+ \to 19^+$
826.9	6521.8	2.7(3)	2.15(30)[f]		$E2$	$18^+ \to 16^+$
874.6	6006.2	0.16(4)		1.11(25)	$M1/E2$	$16^+ \to 15^+$
892.4	8147.0	0.94(5)	2.28(22)[f]		$E2$	$22^+ \to 20^+$
951.8	6521.8	0.16(2)		1.31(22)	$E2$	$18^+ \to 16^+$
966.7	8651.0	0.78(7)	2.13(27)[f]		$E2$	$23^+ \to 21^+$
1030.3	9177.3	0.38(5)		1.49(34)	$E2$	$24^+ \to 22^+$
1046.7	6238.0	1.04(7)	0.46(7)[e]		$M1$	$17^+ \to 16^+$
1092.9	5439.3	1.5(1)	0.92(14)[e]		$E2$	$16^+ \to 14^+$
1093.4	9744.4	0.5(1)		1.27(23)	$E2$	$25^+ \to 23^+$
1106.4	6238.0	0.5(1)	0.93(21)[e]		$E2$	$17^+ \to 15^+$
1166.7	10344.0	0.52(5)		1.51(22)	$E2$	$25^+ \to 23^+$
1221.6	10966.0	0.12(4)			$E2$	$27^+ \to 25^+$
1306.1	11650.1	<0.01			$E2$	$28^+ \to 26^+$
1330.5	6521.8	<0.01			$E2$	$18^+ \to 16^+$
1368.3	12334.3	<0.01			$E2$	$29^+ \to 27^+$
1479.6	5826.0	0.31(2)		1.11(26)	$M1/E2$	$15^+ \to 14^+$
1659.8	6006.2	0.23(2)		1.34(28)	$E2$	$16^+ \to 14^+$
Band D5-chiral						
281.4	7213.0	0.3(1)		1.17(22)	$M1/E2$	$19^+ \to 18^+$
330.0	7543.0	0.42(9)		0.69(15)	$M1$	$20^+ \to 19^+$
384.1	7927.1	0.6(1)		0.71(13)	$M1/E2$	$21^+ \to 20^+$
428.0	8355.1	1.5(5)	1.10(37)[f]		$M1$	$22^+ \to 21^+$
473.0	8828.1	0.5(1)		1.13(24)	$M1/E2$	$23^+ \to 22^+$
519.1	9347.2	0.31(10)			$M1/E2$	$24^+ \to 23^+$
563.9	9911.1	0.10(3)			$M1/E2$	$25^+ \to 24^+$
611.4	7543.0	0.21(10)			$E2$	$20^+ \to 18^+$
670.8	8355.1	0.65(6)	0.93(18)[e]		$M1/E2$	$22^+ \to 21^+$
672.5	7927.1	0.5(2)	1.45(48)[f]		$M1/E2$	$21^+ \to 20^+$
714.1	7927.1	0.18(4)		1.33(40)	$E2$	$21^+ \to 19^+$
812.1	8355.1	0.62(20)		1.4(3)	$E2$	$22^+ \to 20^+$
901.0	8828.1	0.3(1)			$E2$	$23^+ \to 21^+$
975.0	7213.0	0.3(1)		1.33(35)	$E2$	$19^+ \to 17^+$
992.1	9347.2	0.25(10)			$E2$	$24^+ \to 22^+$
1021.2	7543.0	0.6(1)		1.42(21)	$E2$	$20^+ \to 18^+$
1060.7	7927.1	0.8(4)			$E2$	$21^+ \to 19^+$
1083.0	9911.1	0.10(2)			$E2$	$25^+ \to 23^+$

TABLE I. (*Continued.*)

γ-ray energy[a]	E_i (keV)	Intensity[b]	R_{DCO}[c]	R_{ac}[d]	Multipolarity	$J_i^\pi \to J_f^\pi$
1100.5	8355.1	0.2(1)	2.1(6)[f]		E2	$22^+ \to 20^+$
1143.8	8828.1	0.15(5)	1.06(21)[e]		E2	$23^+ \to 21^+$
1156.8	10504.0	<0.01			E2	$26^+ \to 24^+$
1200.2	9347.2	0.4(1)		1.37(28)	E2	$24^+ \to 22^+$
1260.1	9911.1	0.19(4)		1.50(36)	E2	$25^+ \to 23^+$
1326.7	10504.0	0.02(1)			E2	$26^+ \to 24^+$
1371.6	11116.0	<0.01			E2	$27^+ \to 25^+$
Band D6						
315.7	8379.2	0.60(5)	0.35(5)[e]		M1/E2	$22^- \to 21^-$
329.7	8379.2	0.60(4)	0.68(12)[e]		M1/E2	$22^- \to 21^-$
374.0	8753.2	0.82(7)			M1/E2	$23^- \to 22^-$
410.3	9163.5	0.91(8)	0.51(6)[e]		M1	$24^- \to 23^-$
453.7	9617.2	0.49(4)	0.45(7)[e]		M1	$25^- \to 24^-$
491.4	10108.6	0.38(3)	0.28(9)[e]		M1/E2	$26^- \to 25^-$
530.4	10639.0	0.18(2)		0.77(17)	M1	$27^- \to 26^-$
581.2	11220.2	0.07(2)			M1/E2	$28^- \to 27^-$
603.8	11824.0	0.03(1)			M1/E2	$29^- \to 28^-$
660.1	12484.1	0.02(1)			M1/E2	$30^- \to 29^-$
689.7	8753.2	0.10(1)			E2	$23^- \to 21^-$
703.7	8753.2	0.41(3)	0.85(16)[e]		E2	$23^- \to 21^-$
784.3	9163.5	0.22(2)	0.95(14)[e]		E2	$24^- \to 22^-$
864.0	9617.2	0.30(3)	1.10(22)[e]		E2	$25^- \to 23^-$
922.2	8063.5	1.15(6)	0.98(15)[e]		E2	$21^- \to 19^-$
945.1	10108.6	0.52(3)	1.08(13)[e]		E2	$26^- \to 24^-$
1021.8	10639.0	0.32(3)		1.30(21)	E2	$27^- \to 25^-$
1111.6	11220.2	0.17(2)		1.53(28)	E2	$28^- \to 26^-$
1185.0	11824.0	0.10(1)		1.37(36)	E2	$29^- \to 27^-$
1263.9	12484.1	0.08(2)			E2	$30^- \to 28^-$
Band T1						
858.9	7330.7	1.73(16)	1.09(19)[e]		E2	$20^+ \to 18^+$
893.2	8223.9	2.9(3)		1.35(20)	E2	$22^+ \to 20^+$
948.9	9172.8	2.1(1)		1.43(15)	E2	$24^+ \to 22^+$
1018.8	10191.6	1.5(2)		1.42(22)	E2	$26^+ \to 24^+$
1086.8	11278.4	0.92(9)		1.54(20)	E2	$28^+ \to 26^+$
1140.0	12418.4	0.60(10)		1.56(30)	E2	$30^+ \to 28^+$
1121.5	13539.9	0.28(2)		1.39(21)	E2	$32^+ \to 30^+$
1139.6	7330.7	2.0(3)		1.56(30)	E2	$20^+ \to 18^+$
Band T2						
759.5	6184.7	0.58(5)		1.51(27)	E2	$17^- \to 15^-$
826.0	7010.7	0.70(7)		1.46(21)	E2	$19^- \to 17^-$
890.3	7901.0	0.73(8)		1.42(30)	E2	$21^- \to 19^-$
948.6	8849.6	0.7(1)		1.46(27)	E2	$23^- \to 21^-$
1027.4	9877.0	0.67(6)		1.4(2)	E2	$25^- \to 23^-$
1078.8	5425.2	0.65(15)		0.99(29)	E1	$15^- \to 14^+$
1084.0	10961.0	0.6(1)		1.41(25)	E2	$27^- \to 25^-$
1186.9	12147.9	0.44(4)		1.45(20)	E2	$29^- \to 27^-$
1290.9	13438.8	0.36(3)		1.36(34)	E2	$31^- \to 29^-$
1402.6	14841.4	0.22(3)		1.33(27)	E2	$33^- \to 31^-$
1514.0	16355.4	0.09(2)			E2	$(35^-) \to 33^-$
1624.4	17979.8	0.07(2)			E2	$(37^-) \to (35^-)$
1715.3	19695.1	0.03(1)			E2	$(39^-) \to (37^-)$
Band T3						
845.1	9893.5	0.6(1)	1.0(2)[e]		E2	$25^- \to 23^-$
892.4	10785.9	0.42(3)	0.96(10)[e]		E2	$27^- \to 25^-$
998.6	11784.5	0.31(4)		1.4(2)	E2	$29^- \to 27^-$
1099.4	12883.9	0.20(3)	1.08(21)[e]		E2	$31^- \to 29^-$

TABLE I. (*Continued.*)

γ-ray energy[a]	E_i (keV)	Intensity[b]	R_{DCO}[c]	R_{ac}[d]	Multipolarity	$J_i^{\pi} \to J_f^{\pi}$
1188.4	14072.3	0.11(2)	0.93(25)[e]		$E2$	$33^- \to 31^-$
1286.1	15358.3	0.05(1)			$E2$	$(35^-) \to 33^-$
1390.6	16748.9	<0.01			$E2$	$(37^-) \to (35^-)$
Band T4						
606.9	10499.2	0.03(1)			$M1/E2$	$26^- \to 25^-$
860.0	11392.0	0.10(2)			$E2$	$(28^-) \to 26^-$
941.8	10499.2	0.27(2)	0.98(19)[e]		$E2$	$26^- \to 24^-$
973.6	10532.0	0.16(1)		1.44(33)	$E2$	$26^- \to 24^-$
991.6	11490.8	0.23(3)	0.99(16)[e]		$E2$	$28^- \to 26^-$
1022.4	9558.4	0.66(6)	1.11(15)[e]		$E2$	$24^- \to 22^-$
1062.7	12553.5	0.18(3)	0.95(18)[e]		$E2$	$30^- \to 28^-$
1145.1	13698.6	0.11(1)		1.38(20)	$E2$	$32^- \to 30^-$
1226.3	14924.9	0.09(2)			$E2$	$(34^-) \to 32^-$
1301.1	16226.0	0.05(1)			$E2$	$(36^-) \to (34^-)$
1323.3	17549.3	<0.01			$E2$	$(38^-) \to (36^-)$

[a]The error on the transition energies is 0.2 keV for transitions below 1000 keV, 0.5 keV for transitions between 1000 and 1200 keV, and 1 keV for transitions above 1200 keV.

[b]Relative intensities corrected for efficiency, normalized to the intensity of the 373.7 keV transition. The transition intensities were obtained from a combination of total projection and gated spectra.

[c]R_{DCO} has been deduced from an asymmetric γ-γ coincidence matrix sorted with the detectors at 157.6° on one axis, and detectors at $\approx$90° on the other axis. The tentative spin-parity of the states are given in parentheses.

[d]R_{ac} has been deduced from two asymmetric γ-γ coincidence matrices sorted with the detectors at 133.6° and 157.6° on one axis, and detectors at $\approx$90° on the other axis. The tentative spin-parity of the states are given in parentheses.

[e]DCO ratio from spectrum gated on stretched quadrupole transition.

[f]DCO ratio from spectrum gated on stretched dipole transition.

from these spectra, normalized by the different efficiencies of the two sets of detectors, using the formula

$$R_{\mathrm{ac}} = I_\gamma(133.6° + 157.6°)/I_\gamma(75.5° + 104.5°).$$

The typical values for stretched dipole and quadrupole transitions are around 0.8 and 1.4, respectively.

The R_{DCO} values were also extracted from a γ-γ matrix, constructed by sorting prompt coincidence events with the detectors at 157.6° versus those at 75.5° and 104.5°. The DCO ratio is defined as

$$R_{\mathrm{DCO}} = I_\gamma(157.6°, \approx 90°)/I_\gamma(\approx 90°, 157.6°),$$

where $I_\gamma(157.6°, \approx 90°)$ is the intensity of a transition measured by the detectors at 157.6° by gating on the detectors at $\approx$90°, and $I_\gamma(\approx 90°, 157.6°)$ is the intensity of a transition measured by the detectors at $\approx$90° by gating on the detectors at 157.6°. The obtained DCO ratio depends on the multipolarity of the gating transition. The typical R_{DCO} values obtained by gating on a stretched quadrupole transition are $\approx$1 for stretched quadrupole and $\approx$0.46 for dipole transitions, while those obtained by gating on a stretched dipole transition are $\approx$1 for a dipole and $\approx$2.1 for a quadrupole transition.

III. RESULTS AND LEVEL SCHEME

The experimental information on the observed transitions is given in Table I. The level scheme of ^{136}Nd split into three partial level schemes is shown in Figs. 1, 2, and 3. Most of

the observed transitions were grouped in bands: the γ band, two bands of negative parity at low spins (N1–N2), nine bands at medium spin (L1-L9), six bands of dipole transitions (D1–D6) and five chiral partner bands (D1-chiral, D2-chiral, D3-chiral, D4-chiral, D5-chiral) and four high-spin bands (T1–T4). Many states have been newly identified and some previously reported states have been revised.

A. γ band and bands N1, N2

Coincidence spectra obtained by double-gating on selected transitions of the γ band are shown in Fig. 4. The γ band, which was previously known up to $I^\pi = 5^+$ [99], has been extended to higher spins and linked by the 815- and 600-keV transitions to another previously known band built on the 10^+ state at 3768 keV [74]. The γ band is now observed up to $I^\pi = 20^+$: the 895-keV transition on top of the band has been replaced by the 1018-keV transition. Several new transitions of 490, 735, 907, 1163, 1410.7, 1410.8, and 1429 keV have been identified feeding the positive-parity bands L1 and L2, and to the 16^+ state deexcited by the 1093-keV transition. A new 6^+ state has been identified, which decays to the ground-state band (GSB), to the γ band, and to band N1 via the 1252-, 686-, and 192-keV transitions, respectively. The newly identified band N2 decays to the new 6^+ state, to the γ band, and to band N1 via the 366-, 300-, and 154-keV transitions, respectively, and its 6^- and 7^- states are fed by the 412- and 164-keV transitions from band N1. The double-gated
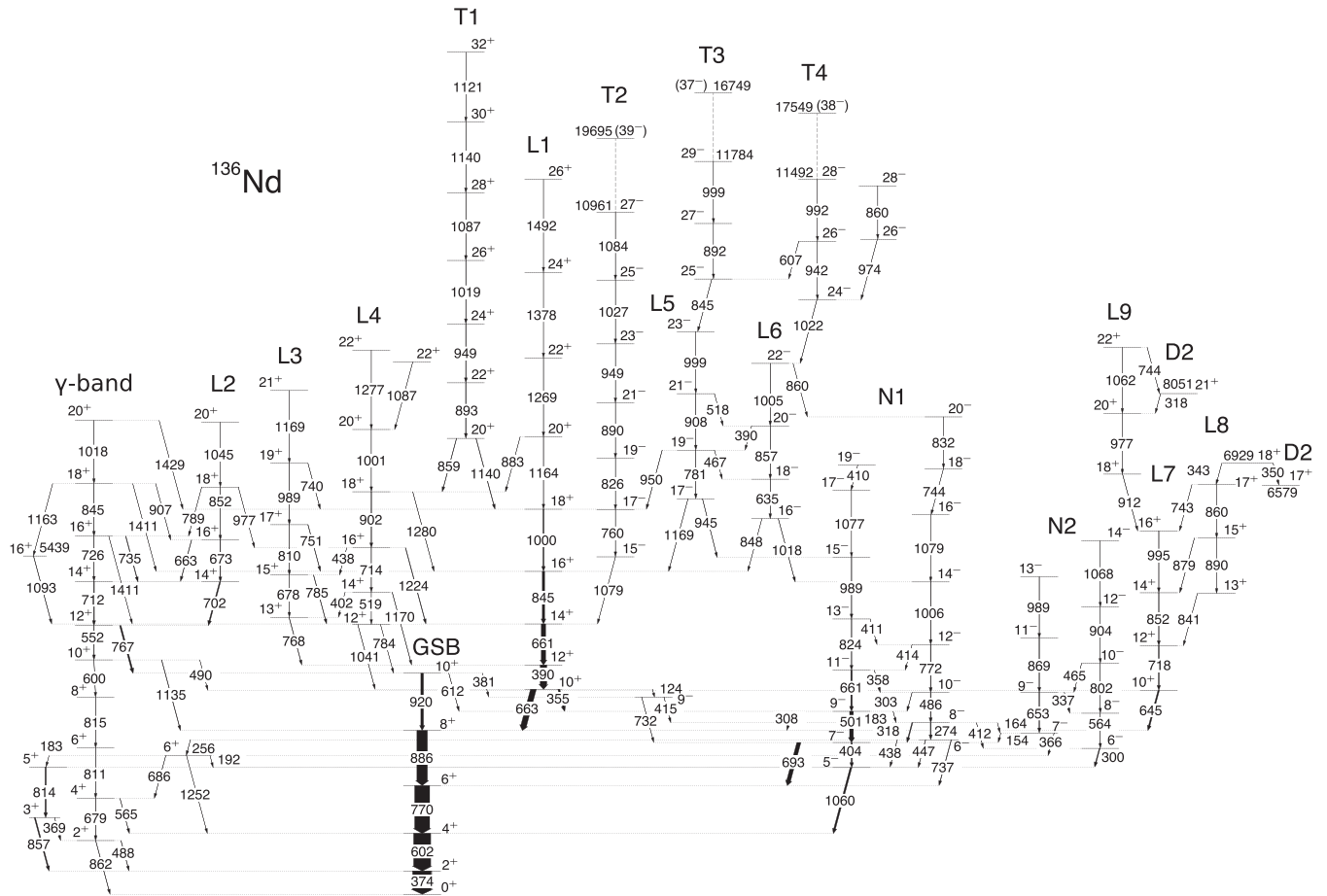
FIG. 1. Partial level scheme of ^{136}Nd showing the low- and medium-spin bands.

spectra given in Fig. 5 show the transitions of band N2. The 1077-, 410-, 1079-, 744-, and 832-keV transitions placed on the top of band N1 are new. We observed two new transitions of 381 and 612 keV from the 10$^+$ state of the GSB towards the intermediate 9$^-$ state, which in turn decays to the 7$^-$ and 8$^-$ states of band N1, and directly towards the 9$^-$ state of band N1, respectively. The bandhead spin of the newly observed band N2 is fixed by the $\Delta I = 1$ transitions with energies of 366 and 300 keV. The negative parity of band N2 is fixed by the 412-keV $E2$ transition connecting the 8$^-$ state of band N1 to the 6$^-$ state of band N2. The negative-parity assignment to band N2 is further supported by the low-energy 154- and 164-keV transitions of $M1/E2$ character between the bands N1 and N2.

B. The medium-spin bands L and T

Band L1 has been extended up to spin $I^\pi = 26^+$, by adding two transitions of 1378 and 1492 keV. Band L2 has been extended up to spin $I^\pi = 20^+$ by a new 1045-keV transition. Four new transition of 663, 735, 789, and 907 keV connecting band L2 to the γ band have been identified. Band L2 also decays via the weak transition of 977 keV to band L4.

Band L3, previously reported in Ref. [44] is confirmed. One new transition of 740 keV connecting the 19$^+$ state with the 18$^+$ state of band L1 has been identified.

Band L4 has been revised due to the newly observed transitions of 519, 1001, 1277 and 1087 keV. It decays via the 438- and 402-keV transitions to band L3, via the 1041-, 1170-, 1224-, and 1280-keV transitions to band L1, and via the 784-keV transition to the GSB. A double-gated spectrum showing the transitions of band L4 is given in Fig. 6.

Bands L5 and L6 previously reported in Ref. [44] are confirmed. Three new transitions of 518, 390, and 467 keV connecting the two bands have been identified. A new transition of 860 keV connects the 22$^-$ state of band L6 to the 20$^-$ state of band N1.

Bands L7 and L8 previously reported in Ref. [44] are confirmed. One in-band transition of 890 keV and one out-of-band transition of 841 keV have been added to band L8. Band L9 is new. It decays to band L7 via the 912-keV transition and is connected to band D2 via the 318- and 744-keV transitions.

Bands T1, T3, and T4 previously reported in Ref. [44] are confirmed, and several new transitions have been identified. A new relatively strong $E2$ transition of 1121 keV has been added on top of band T1 (see Fig. 1). The energies of the highest in-band transitions of bands T3 and T4 have been
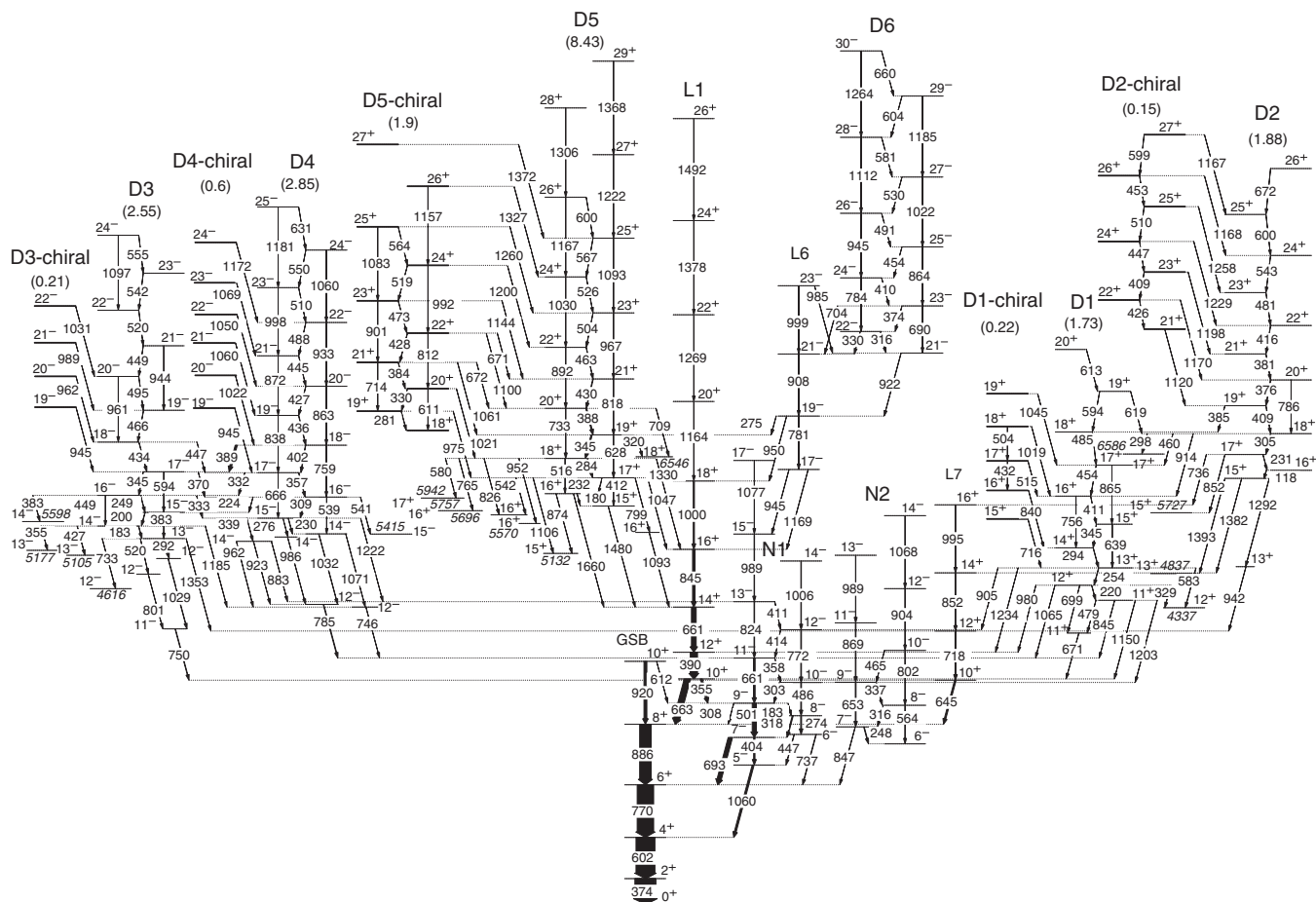
FIG. 2. Partial level scheme of ^{136}Nd showing the dipole bands. The numbers in brackets below the band labels are the relative intensities of the bands.

revised to 1391 and 1323 keV, respectively, whereas the spin and parity of the highest two and three levels, respectively, are tentative.

The newly identified band T2 is built on the 15^- state and decays only to band L1 via the 1079-keV transition. It is observed up to very high spin (39^-). A sum of doubly gated spectra on the in-band transitions of band T2 is given in Fig. 7.

C. The dipole bands

A particular feature of the level scheme of ^{136}Nd is the existence of five pairs of nearly degenerate bands (D1 and D1-chiral, D2 and D2-chiral, D3 and D3-chiral, D4 and D4-chiral, D5 and D5-chiral) and the dipole band D6 without partner. The partial level scheme showing the five pairs of nearly degenerate bands and band D6 is given in Fig. 2.

Band D1, which was first reported in Ref. [77], is confirmed by the present study, but the spins and parity are revised. Three new crossover transitions of 639, 756, and 865 keV, and three new transitions of 485, 594, and 613 keV, placed on top of the previously reported band, have been

identified. Nine new decay-out transitions with energies of 329, 479, 583, 845, 905, 980, 1065, 1203, and 1234 keV have been identified, leading to a bandhead of $I^\pi = 11^+$, with spin $2\hbar$ higher than that previously assigned. The positive parity is assigned based on a series of relatively strong connecting transitions to low-lying states. The new band D1-chiral decays to band D1 via high-energy $E2$ transitions. Double-gated spectra showing the transitions connecting the newly identified band D1-chiral to band D1 are shown in Fig. 8.

Band D2 first reported in Ref. [77] is confirmed, with one new crossover transition of 786 keV. Three new transitions with energies of 385, 460 and 914 keV connect band D2 to band D1. The new band D2-chiral consists of a sequence of six dipole transitions. It decays to band D2 via seven high-energy $E2$ transitions. Double-gated spectra showing the bands D2 and D2-chiral have been recently published in Ref. [9].

Band D3 first reported in Ref. [79] is confirmed, with a revision: one new in-band transition of 449 keV is inserted between the 520- and 495-keV transitions. The two new crossover transitions of 944 and 1097 keV were useful to establish the order of the dipole in-band transitions. The
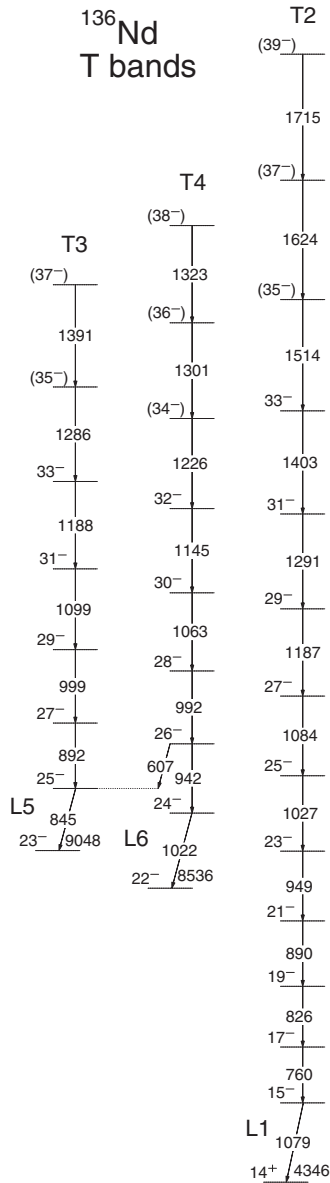
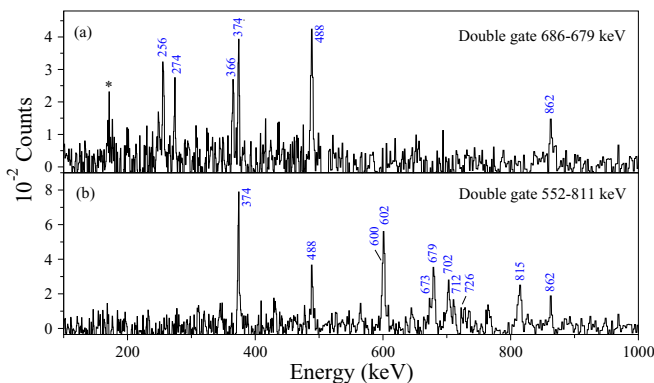FIG. 3. Partial level scheme of ^{136}Nd showing the T bands.

FIG. 4. Double-gated spectra for the γ-band of ^{136}Nd. The peaks corresponding to the γ rays of ^{136}Nd are indicated with their energies, while those of the contaminating transitions are indicated with an asterisk.
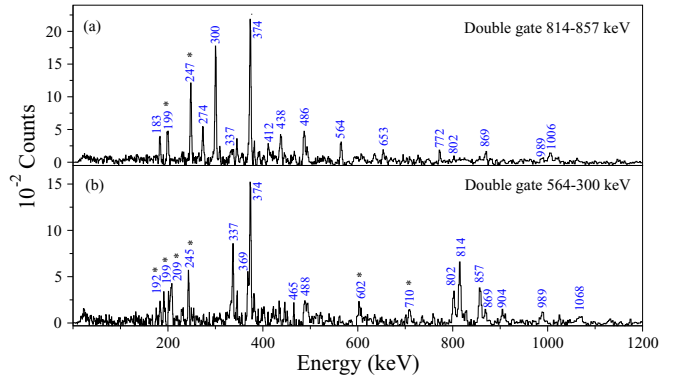

FIG. 5. Double-gated spectra for the band N2 of ^{136}Nd. The peaks corresponding to the contaminating transitions are indicated with asterisks.

band D3-chiral is new. It decays to band D3 via four $E2$ transitions of 945, 962, 989, and 1031 keV. No in-band dipole transitions have been observed in the present data. A double-gated spectrum showing the connecting transitions linking band D3-chiral to band D3 is given in Fig. 9.

Band D4 first reported in Ref. [79] is confirmed, except the last two transitions of 624 and 1173 keV deexciting the 25^- state, which are replaced by the 631- and 1181-keV transitions. A new transition of 541 keV linking the 16^- state of band D4 to the 15^- state of band N1 has also been identified. The band D4-chiral consisting of six levels connected by high-energy transitions to band D4 is new. A spectrum showing these transitions is given in Fig. 10.

Band D5 first reported in Ref. [77] is confirmed. Several new decay-out transitions with energies of 180, 412, 709, 765, 952, 1480, and 1660 keV have been identified. Band D5-chiral consisting of in-band dipole and $E2$ crossover transitions is new. A sum of coincidence spectra obtained by double-gating on the transitions of band D5 is given in Fig. 11. Band D5-chiral is linked to band D5 by many dipole and quadrupole transitions. The relatively large intensities of the transitions of bands D5 and D5-chiral, made possible the extraction of the $B(M1)/B(E2)$ branching ratios for both bands, which are very similar and strongly support the chiral interpretation [9].

Band D6 first reported in Ref. [77] is confirmed. In the present work, we extended it up to spin 30^- by adding on top of the previous band three dipole transitions of 581, 604, and 660 keV, and four crossover transitions of 945, 1112, 1185, and 1264 keV.
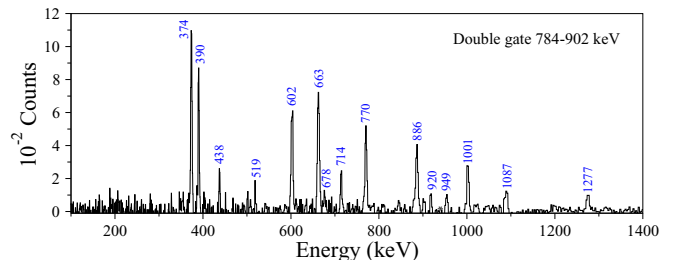

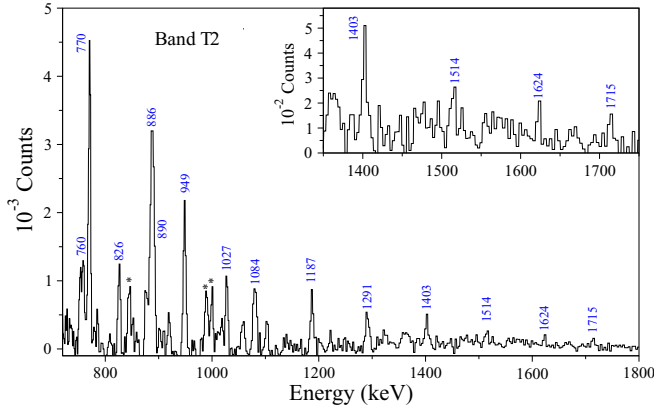FIG. 6. Double-gated spectrum for band L4 of ^{136}Nd.

FIG. 7. Sum of spectra obtained by double-gating on all combinations of in-band transitions of band T2. The peaks corresponding to the contaminating transitions are indicated with asterisks.

D. Search for the isomeric states

Another aim of the present experiment was to search for possible long-lived isomeric states in the populated nuclei, in particular in ^{135}Nd and ^{136}Nd. A γ-time matrix for the focal-plane clovers has been constructed, and is shown in Fig. 12. One can see delayed components of different lengths for the 729-, 884-, and 973-keV transitions below the 10^+, $T_{1/2} = 410$ ns isomer of ^{138}Nd, and for the 640-, 815-, and 948-keV transitions below the 10^+, $T_{1/2} = 308$ ns isomer of ^{134}Ce. We also observed and confirmed the $11/2^-$, $T_{1/2} = 2.7$ μs isomer of ^{137}Pr and the 6^+, $T_{1/2} = 90$ ns isomer of ^{136}Pr, but we could not extract lifetimes more precise than those already known [99]. However, no long-lived isomeric states have been found in ^{135}Nd and ^{136}Nd in the present data.
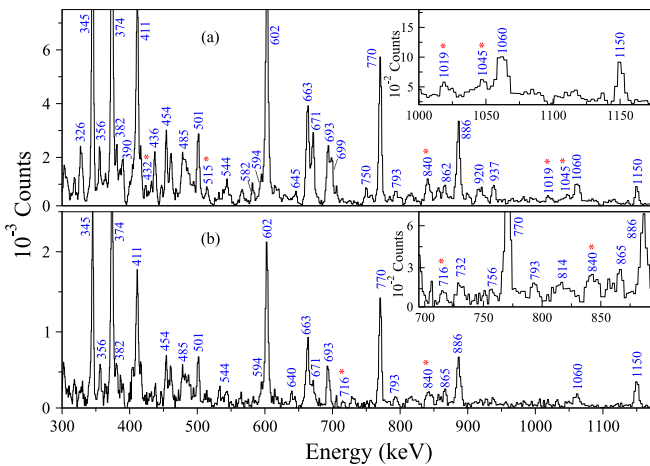

FIG. 8. (a) Sum of spectra obtained by double-gating on all combinations of the 220-, 254- and 294-keV transitions of band D1. (b) Spectrum obtained by double-gating on the 220- and 254-keV transitions of band D1. The peaks corresponding to the in-band transitions of band D1-chiral and to the connecting transitions to band D1 are indicated with asterisks.
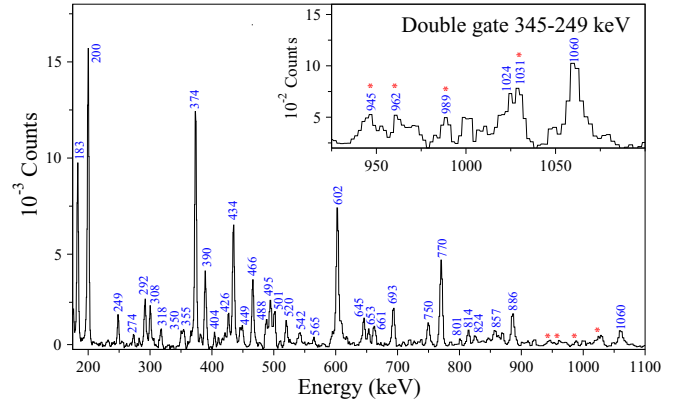

FIG. 9. Double-gated spectrum on the 249- and 345-keV transitions of band D3, showing the connecting transitions of band D3-chiral to band D3, which are indicated with asterisks.

IV. DISCUSSION

The ^{136}Nd nucleus, with 60 protons and 76 neutrons is expected to have a small deformation, $\varepsilon_2 \approx 0.15$–0.20. Thus it is convenient to express the single-particle states in terms of j-shell quantum numbers.

In the CNS formalism the nucleus rotates about one of its principal axes and the pairing is neglected. The deformation is optimized for each single-particle configuration explored. The configurations are labeled by the number of particles in low-j and high-j orbitals, respectively, in the different $\mathcal{N}$ shells. The configurations can be defined relative to a ^{132}Sn core as

$$\pi(g)^{-p_1}(dg)^{p_2}(h_{11/2})^{p_3}\nu(sd)^{-n_1}(h_{11/2})^{-n_2}(hf)^{n_3}(i_{13/2})^{n_4},$$

for which we will use the shorthand notation $[(p_1)p_2p_3, n_1n_2(n_3n_4)]$. The pseudospin partners $d_{5/2}g_{7/2}$ (dg), $s_{1/2}d_{3/2}$ (sd), and $h_{9/2}f_{7/2}$ (hf) are not distinguished in the CNS formalism. Note that all particles are listed, i.e., not only the particles considered as active (unpaired). Note also that the labels do not refer to the pure j shells, but rather to the dominating amplitudes in the Nilsson orbitals. In some cases, for an odd number of particles in a group, the signature will be specified as a subscript $+$ $(\alpha = +1/2)$ or $-$
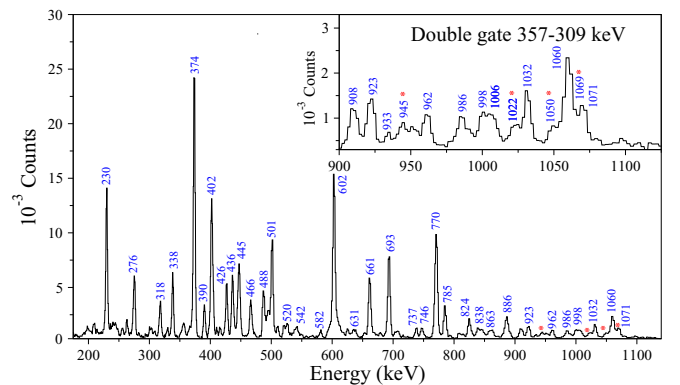

FIG. 10. Double-gated spectrum on the 309- and 357-keV transitions of band D4. The peaks corresponding to the connecting transitions of band D4-chiral to band D4 are indicated with asterisks.
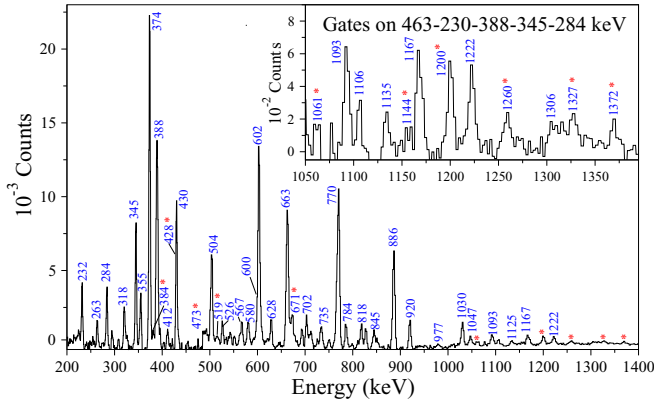
FIG. 11. Sum of spectra obtained by double-gating on all combinations of the 230-, 284-, 345-, 388-, and 463-keV transitions of band D5. The peaks corresponding to the in-band transitions of band D5-chiral and to the connecting transitions to band D5 are indicated with asterisks.

($\alpha = -1/2$). In the present calculations for ^{136}Nd we have used the $A = 130$ parameters [86,87].

The lowest proton configuration has ten protons in the $\pi g_{7/2}$ and $\pi d_{5/2}$ orbitals which are strongly mixed. Higher angular momenta from proton configurations can be obtained by exciting one, two, or three protons from the $\pi g_{7/2}$ and $\pi d_{5/2}$ to the $\pi h_{11/2}$ orbitals. The lowest observed bands have active neutron holes in the $\nu d_{3/2}$ and $\nu s_{1/2}$ orbitals which are also strongly mixed. Higher angular momenta from neutron configurations can be obtained with one, two, or three active holes in the $\nu h_{11/2}$ orbital. Many more excited states and very high angular momenta can be obtained from neutron excitations above the $N = 82$ shell gap into the $\nu f_{7/2}$, $\nu h_{9/2}$ and $\nu i_{13/2}$ orbitals and proton excitations from the $\pi g_{9/2}$ orbital across the $Z = 50$ shell gap.

The level scheme of ^{136}Nd presents a very rich and complex structure at low and medium spins, and several rotational
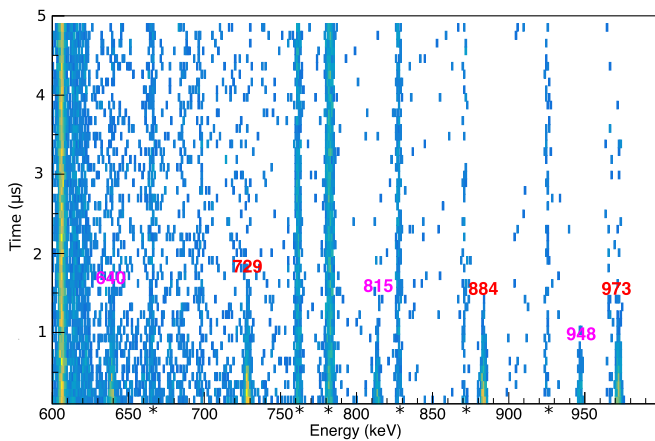

FIG. 12. γ-Time matrix for the clovers at the focal plane. The transitions marked with asterisks represent the β-decay contaminants from the nuclei produced in this experiment: 665 keV, 783 keV, 828 keV and 872 from the β-decay of ^{135}Ce, 761 keV and 925 keV from the β-decay of ^{137}Nd.
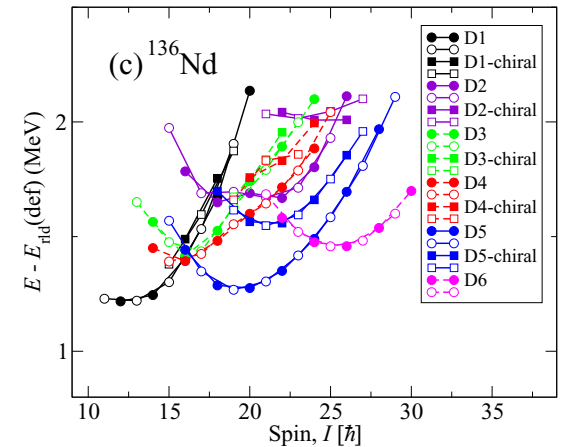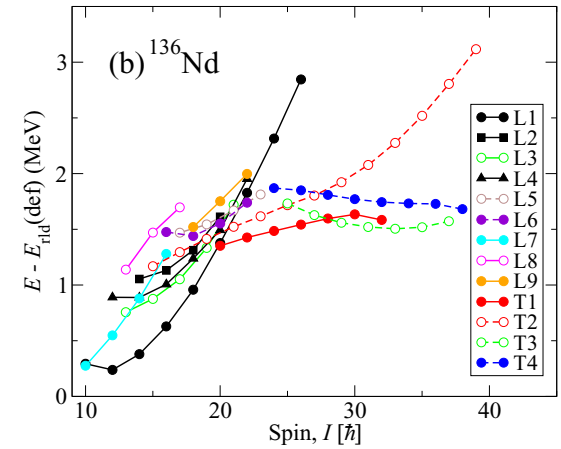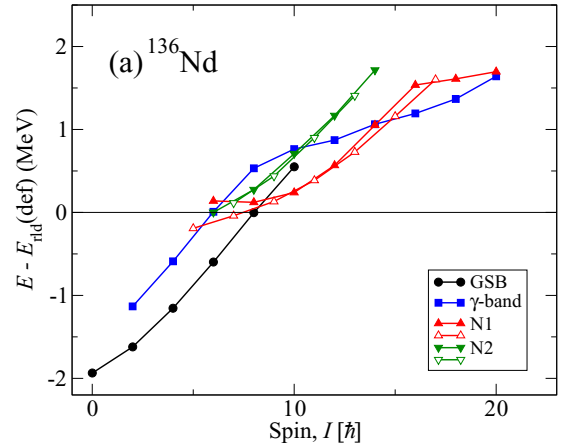

FIG. 13. Energies relative to a standard rotating liquid drop reference calculated for the experimental bands observed in ^{136}Nd. With an odd number of $h_{11/2}$ neutron holes, two signature degenerate bands are formed which are drawn with the same color and filled/open symbols for even/odd spins, respectively.

bands observed up to very high spin. We will discuss here the majority of the observed bands (N, L, D, and T) using the cranked Nilsson-Strutinsky (CNS) model [86–89]. A detailed discussion of the dipole bands in the framework of TAC-CDFT, 3DTAC-CDFT, and Mj-PRM models was published recently [9,10]. In the present work we will discuss the
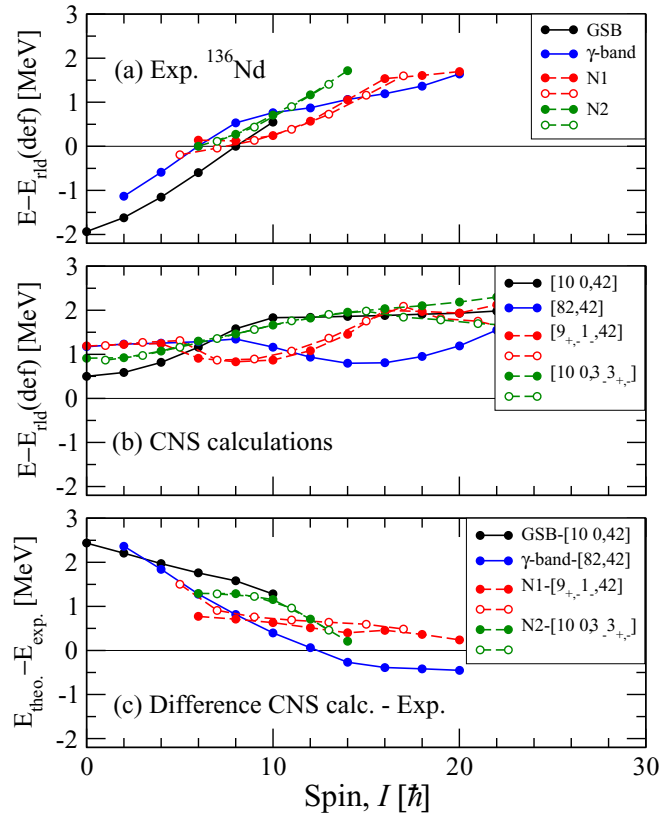
FIG. 14. The observed low-spin bands of ^{136}Nd are shown relative to a rotating liquid drop reference in panel (a), with the calculated configurations assigned to these bands given relative to the same reference in panel (b). Panel (c) provides the difference between calculations and experiment.

FIG. 15. The same as in Fig. 14 but for the medium-spin bands L.

properties of the dipole band configurations resulting from the CNS calculations.

Before discussing the various observed structures, it is instructive to draw the observed bands relative to a rotor reference: the resulting figures reveal not only the relative excitation of the bands, but also details which otherwise are hard to observe in the E-I plots. However, the multitude of bands identified in ^{136}Nd makes their visualization in a single figure cumbersome. We therefore divided them in three groups, which are drawn in the panels of Fig. 13 as follows: the GSB, γ band, and bands N1, N2 in panel (a); the medium- and high-spin bands L and T in panel (b); the five dipole bands D1–D5, their chiral partners D1-chiral to D5-chiral, and band D6 in panel (c).

In panel (a) of Fig. 13 one can see the up-sloping pattern with increasing spin of all the bands, which is induced by the large difference between the moments of inertia of the low-spin bands and that of the rotating liquid drop. One can observe the change of slope of the γ band above spin 10^+, and of the even-spin branch of band N1 above spin 18^+, which are evidently induced by configuration and/or deformation changes.

In panel (b) of Fig. 13 one can observe the yrast nature of band L1 in the spin range $10\hbar$ to $20\hbar$, while just above 10^+ the lowest excited band is L7. There are three positive-parity
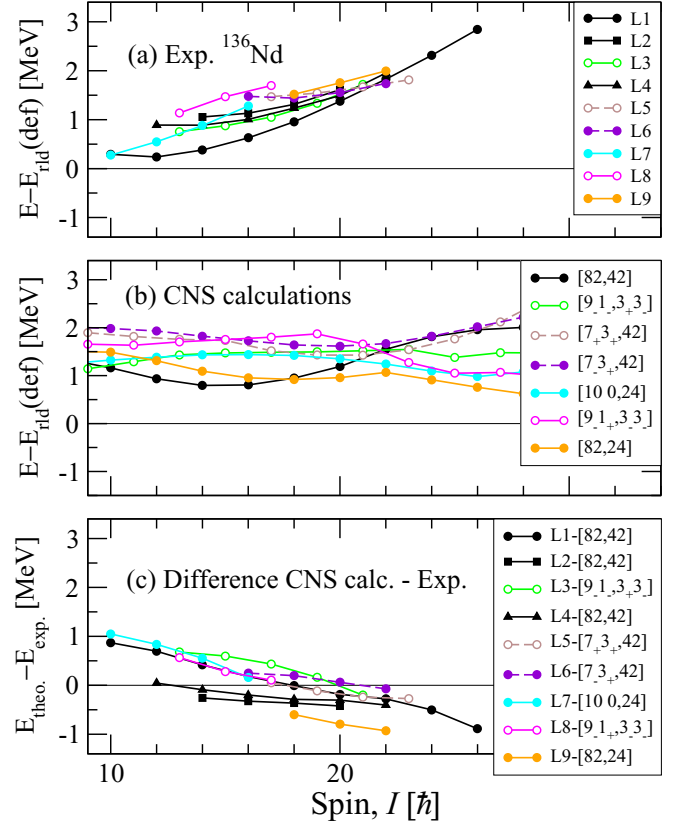
yrare bands L2, L3, and L4, two nearly degenerate negative-parity bands L5 and L6 connected to band L1, and two yrare positive-parity bands L8 and L9 which decay to band L7. At spins higher than 20^+ there are four bands, labeled T1–T4 to emphasize their interpretation in terms of triaxial bands (see the following sections). Band T2 develops over the largest spin interval, from 15^+ to 39^+; at the highest spins it develops up to ≈ 1.7 MeV above yrast, which is a feature similar to that observed in the neighboring ^{137}Nd [70]. The bands T1, T3, and T4 have a nearly flat behavior, with moments of inertia which are similar to that of the liquid drop in the observed spin interval.

In panel (c) of Fig. 13 one can see the well known parabolic behavior of the E-E_{rld} plots, which is induced by the mismatch between the calculated moment of inertia of the drop and that of a given band: for a perfect matching one would have a flat horizontal line (see, e.g., [20]). The chiral doublets are drawn with the same color, but different symbols (circles for the yrast, squares for the yrare bands). The spin of the minimum of each parabola is indicative of the total single-particle spin of the contributing nucleons in the configuration. All bands show nearly degenerate branches with even and odd spins, which indicate the presence in the configurations of one unpaired high-Ω Nilsson orbital. One can observe that the chiral doublets develop only at high spins for the bands D2, D3, D4, that the energy separation is different for the different doublets, and that the chiral doublet observed over the largest spin interval is that of band D5.

TABLE II. Configuration assignments and deformation information for the bands of ^{136}Nd.

Band	Intensity (%)	Parity	CNS Configuration	States	Deformation (ε_2, γ)
GSB	100	+	[10 0,42]	0^+-10^+	($\approx 0.16, \approx -20°$)
γ band	6	+	[82,42]	2^+-20^+	($\approx 0.20, \approx 26°$)
N1	9	−	[$9_{+,-}1_-$,42]	5^--20^-	($\approx 0.18, \approx 25°$)
N2	5	−	[10 0, $3_-3_{+,-}$]	6^--14^-	($\approx 0.16, \approx -25°$)
L1	34	+	[82,42]	10^+-26^+	($\approx 0.20, \approx 25°$)
L2	6	+	[82,42]	14^+-20^+	($\approx 20, \approx 25°$)
L3	2	+	[9_-1_-, 3_+3_-]	13^+-21^+	($\approx 0.16, \approx -25°$)
L4	3	+	[82,42]	12^+-22^+	($\approx 0.20, \approx 25°$)
L5	1.4	−	[7_-3_+,42]	17^--23^-	($\approx 0.20, \approx 25°$)
L6	1.2	−	[7_-3_+,42]	16^--20^-	($\approx 0.20, \approx 20°$)
L7	7.5	+	[10 0,24]	10^+-16^+	($\approx 0.15, \approx -35°$)
L8	0.2	+	[9_-1_+, 3_-3_-]	13^+-18^+	($\approx 0.17, \approx -33°$)
L9	0.7	+	[82,24]	18^+-22^+	($\approx 0.18, \approx 27°$)
T1	3	+	[7_-3_-, 3_-3_-]	20^+-32^+	($\approx 0.18, \approx -35°$)
T2	0.7	−	[82, 3_+3_+]	15^--(39^-)	($\approx 0.19, \approx 26°$)
T3	0.6	−	[82, 3_-3_-]	26^--(37^-)	($\approx 0.17, \approx -30°$)
T4	0.7	−	[7_+3_-,24]	24^--(38^-)	($\approx 0.20, \approx -70°$)
D1	1.7	+	[$9_-1_{+,-}$, 3_+3_3]	11^+-20^+	($\approx 0.18, \approx -25°$)
D2	1.9	+	[7_+3_+, $3_-3_{+,-}$]	15^+-26^+	($\approx 0.20, \approx 21°$)
D3	2.6	−	[82, $3_+3_{+,-}$]	13^--23^-	($\approx 0.20, \approx 25°$)
D4	2.9	−	[82, $3_-3_{+,-}$]	14^--25^-	($\approx 0.20, \approx 25°$)
D5	8.4	+	[82, $3_-3_{+,-}(1_-0)$]	15^+-29^+	($\approx 0.23, \approx 27°$)
D6	1.2	−	[7_+3_+, $3_-3_{+,-}(1_-0)$]	21^--31^-	($\approx 0.23, \approx 25°$)

A. The low- and medium-spin bands

The γ band of ^{136}Nd exhibits a crossing at $I^\pi = 10^+$ similar to that observed in the neighboring ^{134}Nd nucleus [37]. The $B(E2; 2_2^+ \rightarrow 0^+)$ and $B(E2; 2_2^+ \rightarrow 2_1^+)$ values extracted from the relativistic Coulomb excitation measurement reported in Ref. [80] clearly show the large triaxiality ($\gamma \approx 23°$) and pronounced γ softness of ^{136}Nd at low spins. The γ softness is well documented in the $A = 130$ mass region, in particular in the ^{134}Nd nucleus, for which the measured transition probabilities are in good agreement with the O(6) symmetry of the interacting boson model, which is adequate for the description of γ-soft nuclei [100]. Above the crossing at $I^\pi = 10^+$, the γ band exhibits a regular increase of the transition energies as expected for a rotational band, but also several transitions towards the bands L1 and L2, which is a clear indication of mixing with the configurations of these bands. The same behavior of the γ bands has been reported in ^{134}Nd [37]. As one can see in panels (c) of Figs. 14 and 15, the bands L1, L2, L4 and the high-spin part of the γ band are all well reproduced by the [82,42] configuration, which involves a pair of aligned $h_{11/2}$ protons. The calculated deformations in the observed spin range show their enhanced quadrupole deformation ($\varepsilon_2 \approx 0.20$) relative to that of the GSB ($\varepsilon_2 \approx 0.16$), and their pronounced triaxiality $\gamma \approx +25°$ (see Table II).

As one can see Fig. 14, a nice global agreement with the experimental bands N1 and N2 is obtained if one assigns the [$9_{+,-}1_-$, 42] configuration [or $\pi(dg)^1h^1 \otimes \nu 0$ in terms of spherical single-particle orbitals, where $\nu 0$ represents the vacuum for neutrons] to band N1 and the [10 0, $3_-3_{+,-}$] configuration [or $\pi 0 \otimes \nu h^{-1}(sd)^{-1}$ in terms of spherical single-

particle orbitals, where $\pi 0$ represents the vacuum for protons] to band N2. The bands have different deformations, which are induced by the different types of active nucleons: band N1 has higher quadrupole deformation ($\varepsilon_2 \approx 0.18$) than band N2 ($\varepsilon_2 \approx 0.16$), and positive triaxiality ($\gamma \approx +25°$) which is opposite to that of band N2 ($\gamma \approx -25°$). The larger quadrupole deformation and positive triaxiality of band N1 are induced by the low-Ω $h_{11/2}$ proton present in its configuration. The high-Ω $h_{11/2}$ neutron present in the configuration of band N2 induces a smaller increase of the quadrupole deformation and negative triaxiality. Interestingly enough, the high-spin part of band N1, which exhibits a change of slope in the E-E_{rld} plot of Fig. 13, is nicely reproduced by the [$9_{+,-}1_-$, 42] CNS configuration, which shows a jump from the minimum at positive triaxiality ($\varepsilon_2 \approx 0.18$, $\gamma \approx +25°$) to the minimum at negative triaxiality ($\varepsilon_2 \approx 0.17$, $\gamma \approx -85°$), indicating a drastic change of the rotation axis, from the intermediate to the long axis, respectively.

The medium-spin bands L5 and L6 are the continuation of the odd- and even-spin cascades composing band N1. They have the same neutron configuration as band N1 and two additional $h_{11/2}$ aligned protons, which in CNS notation leads to the [$7_{+,-}3_+$, 42] configuration. They have pronounced triaxiality and, as expected due to the presence of three low-Ω $h_{11/2}$ protons, larger quadrupole deformation ($\varepsilon_2 \approx 0.20$) than band N1 ($\varepsilon_2 \approx 0.18$).

Band L7 is based on the [10 0,24] configuration with two $h_{11/2}$ aligned neutrons. It has a smaller deformation ($\varepsilon_2 \approx 0.15$) than the GSB and negative triaxiality ($\gamma \approx -35°$), induced by the presence of two high-Ω $h_{11/2}$ neutrons. The continuation of band L7 to higher spins is band L9, to which we assign the [82,24] configuration involving two $h_{11/2}$
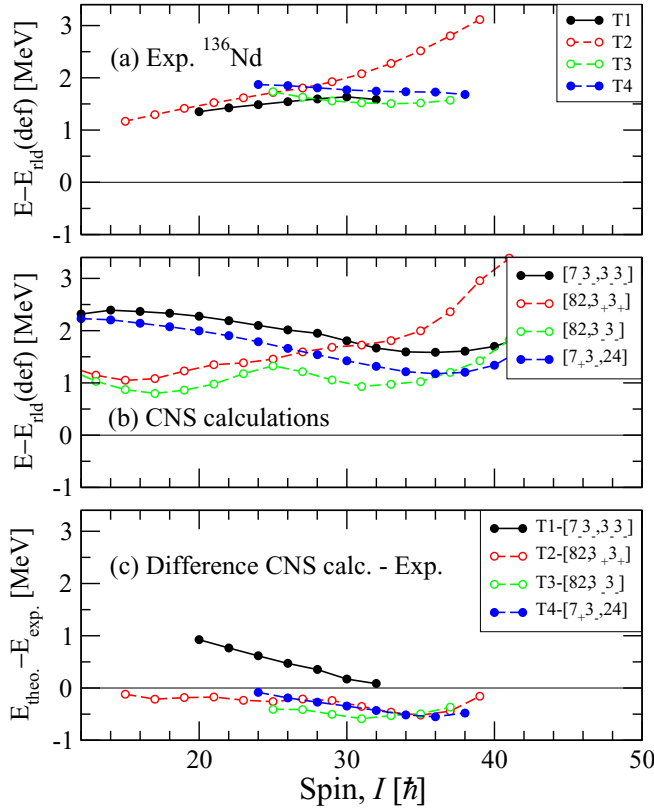
FIG. 16. The same as in Fig. 14 but for the bands T.

FIG. 17. The same as in Fig. 14 but for the bands D.

aligned protons, which induce a larger quadrupole deformation ($\varepsilon_2 \approx 0.18$) and positive triaxiality ($\gamma \approx +27°$). Band L8 has odd spins and is linked to band L7 by weak $\Delta I = 1$ transitions, which most probably have $M1/E2$ character. A possible configuration for band L8 is $[9\_1\_+, 3\_3\_-]$, which is quite different from that of band L7 to which it decays and can explain the weak connecting transitions.

B. The T bands

In the high-spin region we observed four bands that are called T bands to underline their pronounced triaxiality, which distinguish them from the other high-spin bands based on nearly axial shapes and are dominated by highly-deformed (HD) configurations. Band T1 decays only to bands L1 and L4, which are well reproduced by the [82,42] configuration involving two $h_{11/2}$ aligned protons. As it is not linked through several transitions to the other bands, one reasonably can assume that its configuration is quite different from the configurations of the medium-spin bands. One possible configuration is $[7\_3\_-, 3\_3\_-]$, which involves one $h_{11/2}$ proton and one $h_{11/2}$ neutron.

The band T2 is observed over a wide spin range from $I = 15$ to $I = 39$, and decays only to band L1. Its increasing excitation energy relative to the other high-spin bands (see Figs. 13 and 16) is an intriguing behavior that was recently observed in a band in the neighboring ^{137}Nd nucleus [70] and interpreted in terms of rotation of an oblate shape. A possible configuration for band T2 of ^{136}Nd is $[82, 3\_+3\_+]$, which
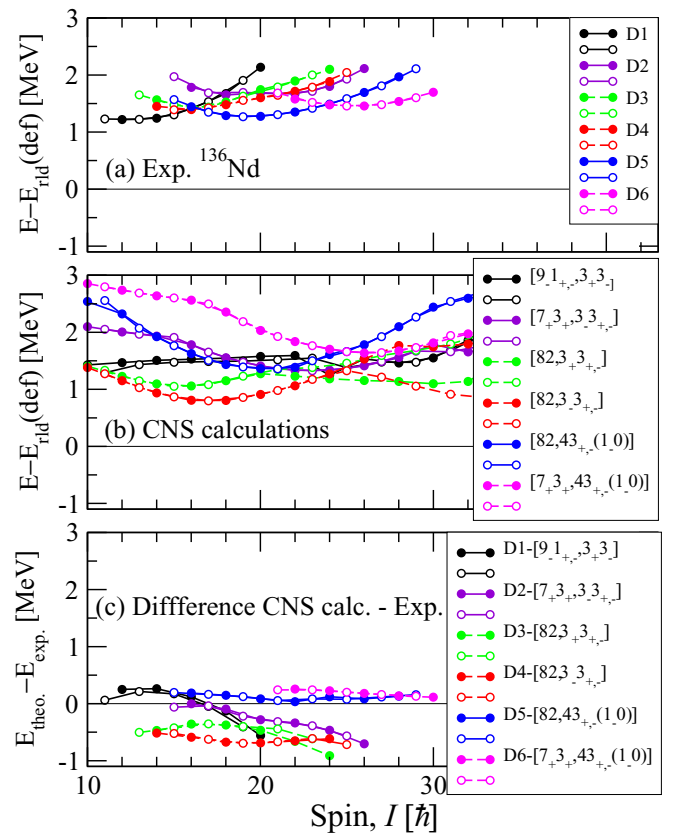
involves one more neutron in the $h_{11/2}$ orbital. The calculated deformation is ($\varepsilon_2 \approx 0.19$, $\gamma \approx +26°$) up to $I^\pi = 19^-$, while in the range $I^\pi = 21^-$ to $I^\pi = 39^-$ the deformation changes gradually from ($\varepsilon_2 \approx 0.17$, $\gamma \approx -20°$) to ($\varepsilon_2 \approx 0.09$, $\gamma \approx -54°$). This decreasing quadrupole deformation and increase of the triaxiality with increasing spin is a behavior similar to band O of ^{137}Nd [70].

The bands T3 and T4 have possible configurations $[82, 3\_3\_-]$ and $[7\_+3\_-, 24]$, respectively. Their quadrupole deformations decrease gradually with increasing spin at quasiconstant triaxiality, from ($\varepsilon_2 \approx 0.20$, $\gamma \approx -70°$) to ($\varepsilon_2 \approx 0.12$, $\gamma \approx -68°$) for band T3, and from ($\varepsilon_2 \approx 0.17$, $\gamma \approx -30°$) to ($\varepsilon_2 \approx 0.12$, $\gamma \approx 45°$) for band T4.

C. The dipole bands

The CNS configurations assigned to the dipole bands of ^{136}Nd are shown in Fig. 17, and are in global agreement with those calculated with the CDFT model in Ref. [10]. Of course, only the configurations of the yrast partners of the chiral doublets can be described by the CNS model, which assumes the rotation around one of the principal axes. As one can see in Table II, all dipole bands D1–D6 have a pronounced triaxiality, close to the maximum of $30°$. The calculated triaxiality is positive for all bands excepting for band D1. The configuration assignment is quite straightforward, being based on the measured energies, spin-parities, and decay patterns. The configuration assignments are as follows:

(1) Band D1, having positive parity, decays to band L7 and the bottom of band L1, which are based on $\nu h_{11/2}^2$ and $\pi h_{11/2}^2$ configurations, respectively. The assigned $[9_{-1_{+,-}}, 3_{+}3_{-}]$ configuration is the simplest single-particle excitation leading to a low-lying positive-parity band, which, however, maintains one low-Ω proton and one high-Ω neutron in the $h_{11/2}$ orbitals to assure the perpendicular geometry of the angular momenta required by dipole and chiral bands.

(2) Band D2, having positive parity, develops above spin $I = 15^+$ and has a fragmented decay to many low-lying bands, including band D1. A two-quasiparticle excitation with respect to band D1 appears as the natural choice, and we therefore assign the $[7_{+}3_{+}, 3_{-}3_{+,-}]$ configuration, involving two additional $h_{11/2}$ protons relative to band D1.

(3) Bands D3 and D4, having negative parity, are connected through several transitions and decay via a multitude of transitions towards the low-lying bands. Their spins and excitation energies are similar to those of band D2. The most probable configurations are $[82, 3_{+}3_{+,-}]$ and $[82, 3_{-}3_{+,-}]$, which are in good agreement with experiment.

(4) Band D5 is the strongest dipole band, has positive parity, and decays mainly to band L1. Its properties are nicely reproduced by the $[82, 43_{+,-}(1_{-}0)]$ configuration which involves one neutron in the intruder $(h_{9/2}, f_{7/2})$ orbital. As a consequence, its quadrupole deformation is larger ($\varepsilon_2 \approx 0.23$) than those of bands D1–D4, due to the polarizing force of the $(h_{9/2}, f_{7/2})$ intruder orbital.

(5) Band D6 is the highest excited dipole band, has negative parity, and decays to band L6. We assign it the $[7_{+}3_{+}, 43_{+,-}(1_{-}0)]$ configuration, which has one neu-

tron excited from the $h_{11/2}$ to the $(h_{9/2}, f_{7/2})$ intruder orbital relative to band L6.

V. SUMMARY

Summarizing, we performed a study of the triaxial nucleus ^{136}Nd up to very high spin. The configuration assignment is based on CNS calculations. Five pairs of chiral pairs of rotational bands were identified in ^{136}Nd. It is the first time that chiral bands have been observed in an even-even nucleus. The present work aims to the complete spectroscopy of ^{136}Nd, which, based on the present experimental information, is known in detail from low to very high spins, being one of the best studied nuclei in the $A = 130$ mass region.

[1] P. Möller, R. Bengtsson, B. G. Carlsson, P. Olivius, and T. Ichikawa, Phys. Rev. Lett. **97**, 162502 (2006).

[2] S. Frauendorf and J. Meng, Nucl. Phys. A **617**, 131 (1997).

[3] B. W. Xiong and Y. Y. Wang, At. Data Nucl. Data Tables **111-112** (2018), doi:10.1016/j.adt.2018.05.002.

[4] J. Meng, J. Peng, S. Q. Zhang, and S.-G. Zhou, Phys. Rev. C **73**, 037303 (2006).

[5] J. Peng, H. Sagawa, S. Q. Zhang, J. M. Yao, Y. Zhang, and J. Meng, Phys. Rev. C **77**, 024309 (2008).

[6] J. M. Yao, B. Qi, S. Q. Zhang, J. Peng, S. Y. Wang, and J. Meng, Phys. Rev. C **79**, 067302 (2009).

[7] J. Li, S. Q. Zhang, and J. Meng, Phys. Rev. C **83**, 037301 (2011).

[8] A. D. Ayangeakaa *et al.*, Phys. Rev. Lett. **110**, 172504 (2013).

[9] C. M. Petrache *et al.*, Phys. Rev. C **97**, 041304(R) (2018).

[10] Q. B. Chen, B. F. Lv, C. M. Petrache, and J. Meng, Phys. Lett. B **782**, 744 (2018).

[11] J. T. Matta *et al.*, Phys. Rev. Lett. **114**, 082501 (2015).

[12] S. Frauendorf and F. Dönau, Phys. Rev. C **89**, 014322 (2014).

[13] K. Tanabe and K. Sugawara-Tanabe, Phys. Rev. C **95**, 064315 (2017).

[14] C. M. Petrache, I. Ragnarsson, H.-L. Ma, R. Leguillon, T. Zerrouki, D. Bazzacco, and S. Lunardi, Phys. Rev. C **91**, 024302 (2015).

[15] C. M. Petrache *et al.*, Phys. Rev. C **93**, 064305 (2016).

[16] C. M. Petrache *et al.*, Phys. Rev. C **94**, 064309 (2016).

[17] A. D. Ayangeakaa, U. Garg, C. M. Petrache, S. Guo, P. W. Zhao, J. T. Matta, B. K. Nayak, D. Patel, R. V. F. Janssens, M. P. Carpenter, C. J. Chiara, F. G. Kondev, T. Lauritsen, D. Seweryniak, S. Zhu, S. S. Ghugre, and R. Palit, Phys. Rev. C **93**, 054317 (2016).

[18] C. M. Petrache, S. Frauendorf, M. Matsuzaki, R. Leguillon, T. Zerrouki, S. Lunardi, D. Bazzacco, C. A. Ur, E. Farnea, C. Rossi Alvarez, R. Venturelli, and G. de Angelis, Phys. Rev. C **86**, 044321 (2012).

[19] C. M. Petrache, I. Ragnarsson, H.-L. Ma, R. Leguillon, T. Konstantinopoulos, T. Zerrouki, D. Bazzacco, and S. Lunardi, Phys. Rev. C **88**, 051303 (2013).

[20] C. M. Petrache *et al.*, Phys. Rev. C **61**, 011305(R) (1999).

[21] S. Bhowal *et al.*, Phys. Rev. C **84**, 024313 (2011).

[22] R. Leguillon, C. M. Petrache, T. Zerrouki, T. Konstantinopoulos, K. Hauschild, A. Korichi, A. Lopez-Martens, S. Frauendorf, I. Ragnarsson, P. T. Greenlees, U. Jakobsson, P. Jones, R. Julin, S. Juutinen, S. Ketelhut, M. Leino, P. Nieminen, M.

Nyman, P. Peura, P. Rahkila, P. Ruotsalainen, M. Sandzelius, J. Saren, C. Scholey, J. Sorri, J. Uusitalo, H. Hübel, A. Neußer-Neffgen, A. Al-Khatib, A. Bürger, N. Nenoff, A. K. Singh, D. Curien, G. B. Hagemann, B. Herskind, G. Sletten, P. Fallon, A. Görgen, P. Bednarczyk, and D. M. Cullen, Phys. Rev. C **88**, 014323 (2013).

[23] C. M. Petrache *et al.*, Phys. Rev. C **72**, 064318 (2005).

[24] T. Zerrouki, C. Petrache, R. Leguillon, K. Hauschild, A. Korichi, A. Lopez-Martens, S. Frauendorf, I. Ragnarsson, H. Hübel, A. Neußer-Neffgen, A. Al-Khatib, P. Bringel, A. Bürger, N. Nenoff, G. Schönwaßer, A. Singh, D. Curien, G. Hagemann, B. Herskind, G. Sletten, P. Fallon, A. Görgen, and P. Bednarczyk, Eur. Phys. J. A **51**, 50 (2015).

[25] C. M. Petrache *et al.*, Phys. Rev. C **92**, 034314 (2015).

[26] A. Neusser *et al.*, Phys. Rev. C **70**, 064315 (2004).

[27] D. J. Hartley *et al.*, Phys. Rev. C **63**, 024316 (2001).

[28] D. J. Hartley *et al.*, Phys. Rev. C **60**, 041301 (1999).

[29] C. M. Petrache *et al.*, Phys. Lett. B **223**, 223 (1997).

[30] D. T. Joss *et al.*, Phys. Rev. C **54**, 969(R) (1996).

[31] D. Bazzacco *et al.*, Phys. Rev. C **58**, 2002 (1998).

[32] R. Wadsworth *et al.*, J. Phys. G **13**, L207 (1987).

[33] S. M. Mullins *et al.*, Phys. Rev. C **45**, 2683 (1992).

[34] S. A. Forbes *et al.*, Z. Phys. A **352**, 15 (1995).

[35] F. G. Kondev *et al.*, Phys. Rev. C **60**, 011303 (1999).

[36] C. M. Petrache *et al.*, Phys. Lett. B **335**, 307 (1994).

[37] C. M. Petrache *et al.*, Phys. Lett. B **387**, 31 (1996).

[38] C. M. Petrache *et al.*, Phys. Rev. C **57**, 10(R) (1998).

[39] C. M. Petrache, Z. Phys. A **358**, 225 (1997).

[40] E. M. Beck *et al.*, Phys. Rev. Lett. **58**, 2182 (1987).

[41] M. A. Deleplanque *et al.*, Phys. Rev. C **52**, 2302(R) (1995).

[42] P. Willsau *et al.*, Phys. Rev. C **48**, 494(R) (1993).

[43] R. M. Clark *et al.*, Phys. Lett. B **343**, 59 (1995).

[44] C. M. Petrache *et al.*, Phys. Lett. B **373**, 275 (1996).

[45] S. Perries *et al.*, Phys. Rev. C **60**, 064313 (1999).

[46] C. M. Petrache *et al.*, Nucl. Phys. A **617**, 228 (1997).

[47] C. M. Petrache *et al.*, Phys. Lett. B **219**, 145 (1996).

[48] S. Lunardi, R. Venturelli, D. Bazzacco, C. M. Petrache, C. Rossi-Alvarez, G. de Angelis, G. Vedovato, D. Bucurescu, and C. Ur, Phys. Rev. C **52**, 6(R) (1995).

[49] S. Lunardi *et al.*, Phys. Rev. C **69**, 054302 (2004).

[50] A. Galindo-Uribarri *et al.*, Phys. Rev. C **54**, 454(R) (1996).

[51] A. T. Semple *et al.*, J. Phys. G **24**, 1125 (1998).

[52] J. N. Wilson *et al.*, Phys. Rev. C **55**, 519 (1997).

[53] Y. X. Luo, J. Q. Zhong, D. J. G. Love, A. Kirwan, P. J. Bishop, M. J. Godfrey, I. Jenlkins, P. J. Nolan, S. M. Mullins, and R. Wadsworth, Z. Phys. A **329**, 125 (1988).

[54] A. T. Semple *et al.*, Phys. Rev. C **54**, 425 (1996).

[55] E. S. Paul *et al.*, Phys. Rev. C **71**, 054309 (2005).

[56] D. Santos *et al.*, Phys. Rev. Lett. **74**, 1708 (1995).

[57] K. Hauschild *et al.*, Phys. Lett. B **353**, 438 (1995).

[58] N. J. O'Brien, A. Galindo-Uribarri, V. P. Janzen, D. T. Joss, P. J. Nolan, C. M. Parry, E. S. Paul, D. C. Radford, R. Wadsworth, and D. Ward, Phys. Rev. C **59**, 1334 (1999).

[59] R. M. Clark *et al.*, Phys. Rev. Lett. **76**, 3510 (1996).

[60] Y. He *et al.*, J. Phys. G **16**, 657 (1990).

[61] S. M. Mullins *et al.*, Phys. Lett. B **312**, 272 (1993).

[62] A. J. Kirwan, G. C. Ball, P. J. Bishop, M. J. Godfrey, P. J. Nolan, D. J. Thornley, D. J. G. Love, and A. H. Nelson, Phys. Rev. Lett. **58**, 467 (1987).

[63] K. Hauschild *et al.*, Phys. Rev. C **52**, 2281(R) (1995).

[64] E. S. Paul, D. B. Fossan, Y. Liang, R. Ma, and N. Xu, Phys. Rev. C **40**, 1255 (1989).

[65] R. Ma, E. S. Paul, D. B. Fossan, Y. Liang, N. Xu, R. Wadsworth, I. Jenkins, and P. J. Nolan, Phys. Rev. C **41**, 2624 (1990).

[66] E. S. Paul, D. B. Fossan, Y. Liang, R. Ma, N. Xu, R. Wadsworth, I. Jenkins, and P. J. Nolan, Phys. Rev. C **41**, 1576 (1990).

[67] S. J. Zhu, L. Y. Zhu, M. Li, C. Y. Gan, M. Sakhaee, L. M. Yang, R. Q. Xu, Z. Zhang, Z. Jiang, G. L. Long, S. X. Wen, X. G. Wu, and X. A. Liu, Phys. Rev. C **62**, 044310 (2000).

[68] P. H. Regan, G. D. Dracoulis, A. P. Byrne, G. J. Lane, T. Kibedi, P. M. Walker, and A. M. Bruce, Phys. Rev. C **51**, 1745 (1995).

[69] E. S. Paul, S. Shi, C. W. Beausang, D. B. Fossan, R. Ma, W. F. Piel, Jr., N. Xu, and P. K. Weng, Phys. Rev. C **36**, 2380 (1987).

[70] C. M. Petrache *et al.* (unpublished).

[71] D. Habs, H. Klewe-Nebenius, R. Löhken, S. Göring, J. van Klinken, H. Rebel, and G. Schatz, Z. Phys. **250**, 179 (1972).

[72] M. M. Aléonard, Y. E. Masri, I. Y. Lee, F. S. Stephens, M. A. Deleplanque, and R. M. Diamond, Nucl. Phys. A **350**, 190 (1980).

[73] V. Barci, H. El-Samman, A. Gizon, J. Gizon, R. Kossakowski, B. M. Nyako, T. Vertse, S. Elfström, D. Jerrestam, W. Klamra, T. Lindblad, and T. Bengtsson, Z. Phys. A **325**, 399 (1986).

[74] E. S. Paul, C. W. Beausang, D. B. Fossan, R. Ma, W. F. Piel, Jr., P. K. Weng, and N. Xu, Phys. Rev. C **36**, 153 (1987).

[75] J. Billowes, K. P. Lieb, J. W. Noe, W. F. Piel, Jr., S. L. Rolston, G. D. Sprouse, O. C. Kistner, and F. Christancho, Phys. Rev. C **36**, 974 (1987).

[76] E. M. Beck, R. J. McDonald, A. O. Macchiavelli, J. C. Bacelar, M. A. Deleplanque, R. M. Diamond, J. E. Draper, and F. S. Stephens, Phys. Lett. B **195**, 531 (1987).

[77] C. M. Petrache *et al.*, Phys. Rev. C **53**, 2581(R) (1996).

[78] S. Mukhopadhyay *et al.*, Phys. Rev. C **78**, 034311 (2008).

[79] E. Mergel *et al.*, Eur. Phys. J. A **15**, 417 (2002).

[80] T. Saito *et al.*, Phys. Lett. B **669**, 19 (2008).

[81] G. L. Long, Phys. Rev. C **55**, 3163 (1997).

[82] D. Vretenar, S. Brant, G. Bonsignori, L. Corradini, and C. M. Petrache, Phys. Rev. C **57**, 675 (1998).

[83] K. Tanabe and K. Sugawara-Tanabe, Phys. Lett. B **259**, 12 (1991).

[84] L. Próchniak, K. Zajac, K. Pomorski, S. G. Rohoziński, and J. Srebrny, Nucl. Phys. A **648**, 181 (1999).

[85] J. A. Sheikh, G. H. Bhat, R. Palit, Z. Naik, and Y. Sun, Nucl. Phys. A **824**, 58 (2009).

[86] A. Afanasjev, D. Fossan, G. Lane, and I. Ragnarsson, Phys. Rep. **322**, 1 (1999).

[87] T. Bengtsson and I. Ragnarsson, Nucl. Phys. A **436**, 14 (1985).

[88] B. G. Carlsson and I. Ragnarsson, Phys. Rev. C **74**, 011302 (2006).

[89] A. Afanasjev and I. Ragnarsson, Nucl. Phys. A **591**, 387 (1995).

[90] P. J. Nolan, F. A. Beck, and D. B. Fossan, Annu. Rev. Nucl. Part. Sci. **99**, 561 (1994).

[91] M. Leino *et al.*, Nucl. Instrum. Methods Phys. Res. A **99**, 653 (1995).

[92] R. D. Page *et al.*, Nucl. Instrum. Methods Phys. Res. A **204**, 634 (2003).

[93] I. H. Lazarus, D. E. Appelbe, P. A. Butler, P. J. Coleman-Smith, J. R. Cresswell, S. J. Freeman, R. D. Herzberg, I. Hibbert, D. T. Joss, S. C. Letts *et al.*, IEEE Trans. Nucl. Sci. **48**, 567 (2001).

[94] P. Rahkila, Nucl. Instrum. Methods Phys. Res. A **595**, 637 (2008).

[95] D. Radford, Nucl. Instrum. Methods Phys. Res. A **361**, 297 (1995).

[96] D. Radford, Nucl. Instrum. Methods Phys. Res. A **361**, 306 (1995).

[97] A. Krämer-Flecken, T. Morek, R. M. Lieder, W. Gast, G. Hebbinghaus, H. M. Jäger, and W. Urban, Nucl. Instrum. Methods Phys. Res. A **275**, 333 (1989).

[98] C. J. Chiara *et al.*, Phys. Rev. C **75**, 054305 (2007).

[99] ENSDF database, NNDC Online Data Service, http://www.nndc.bnl.gov/ensdf/.

[100] T. Klemme *et al.*, Phys. Rev. C **60**, 034301 (1999).